DEVELOPMENT AND EXPERIMENTAL CHARACTERIZATION OF A 532 nm SHG SOURCE FOR SQUEEZED LIGHT APPLICATIONS

M.Tech. Thesis

By

BISWAJEET MISHRA

DEPARTMENT OF MECHANICAL ENGINEERING

INDIAN INSTITUTE OF TECHNOLOGY INDORE

MAY 2025

DEVELOPMENT AND EXPERIMENTAL CHARACTERIZATION OF A 532 nm SHG SOURCE FOR SQUEEZED LIGHT APPLICATIONS

A THESIS

submitted in partial fulfillment of the
requirements for the award of the degree
of
Master of Technology

by

BISWAJEET MISHRA

DEPARTMENT OF MECHANICAL ENGINEERING
INDIAN INSTITUTE OF TECHNOLOGY INDORE

MAY 2025

INDIAN INSTITUTE OF TECHNOLOGY INDORE

CANDIDATE'S DECLARATION

I hereby certify that the work which is being presented in the thesis entitled **DEVELOPMENT AND EXPERIMENTAL CHARACTERIZATION OF A 532 nm SHG SOURCE FOR SQUEEZED LIGHT APPLICATIONS**, in partial fulfillment of the requirements for the award of the degree of **MASTER OF TECHNOLOGY** and submitted in the **DISCIPLINE OF MECHANICAL ENGINEERING**, Indian Institute of Technology Indore, is an authentic record of my own work carried out during the time period from **June 2024** to **May 2025**, under the supervision of **Dr. Jogy George, SO/H, ALOD, RRCAT** and **Prof. Abhirup Datta, Head, DAASE, IIT Indore**.

The matter presented in this thesis has not been submitted by me for the award of any other degree of this or any other institute.

Biswajeet Mishra 22/05/2025

Signature of the student with date
(BISWAJEET MISHRA)

This is to certify that the above statement made by the candidate is correct to the best of my/our knowledge.

JGeorge 22/5/2025

Signature of the Supervisor of M.Tech. thesis #1 (with date)
(DR. JOGY GEORGE)

Signature of the Supervisor of M.Tech. thesis #2 (with date)
(PROF. ABHIRUP DATTA)

BISWAJEET MISHRA has successfully given his **M.Tech. Oral Examination** held on **9th May 2025**.

JGeorge 22/5/2025

Signature(s) of Supervisor(s) of M.Tech. thesis
Date:

Convener, DPGC
Date: 23-05-25

Signature of PSPC Member #1
Date:

Signature of PSPC Member #2
Date:

ACKNOWLEDGEMENTS

I would like to express my deepest gratitude to my supervisors, Dr. Jogy George and Prof. Abhirup Datta, for their invaluable guidance, encouragement, and continuous support throughout the course of this work. Their insights and expertise have been instrumental in shaping the direction and quality of this research.

I am especially thankful to Shri Mohammad Khursheed, whose constant support, involvement, and technical guidance throughout this work have been no less than that of a co-guide.

I also wish to sincerely thank Dr. Sendhil Raja S., Head of the Advanced Laser and Optics Division (ALOD), for providing me the opportunity to work in ALOD and for his strong support and leadership. His efforts in fostering a collaborative and resourceful research environment were invaluable to the progress of this work.

I extend my sincere thanks to Shri Pradeep Kumar, Shri Subhamoy Chakraborty, Dr. Yogesh Verma, Shri Brijesh Pant, Shri Pramod Mahto, Shri L. N. Birla, Shri Ranjeev Kumar Choudhary, Shri Sharad Kumar, Shri Sunil Kumar, Shri Sivananda Reddy, Shri Rohan Bhandare and all the members of the Advanced laser and Optics division (ALOD) for their assistance, insightful discussions, and for providing a stimulating and collaborative environment. Their support has been invaluable throughout various stages of this project.

I also gratefully acknowledge Prof. Manoneeta Chakraborty and Prof. Suman Majumdar from IIT Indore for their kind support and encouragement throughout the course of this work.

I sincerely thank my friends Naveen Kumar, Prabhat Kumar Dhurve, K. K. Malakar, Rushikesh Mali, Vivek Ranjan Singh, Bittu Kumar, Shubhi Tiwari, Himanshu Sharma, Shruti Sharma, Anuj Mishra, and Suryaprakash for being a source of joy, perspective, and occasional distraction when I needed it most. Their companionship made this journey not just bearable, but genuinely enjoyable.

Finally, I am grateful to everyone who contributed, directly or indirectly, to the successful completion of this work.

Abstract

The objective of this project is to design and develop a second-harmonic generation (SHG) source at 532 nm for the generation of squeezed light at 1064 nm. To achieve 5 dB of squeezing, a pump power of approximately 2 mW at 532 nm is required. Our goal is to generate more than 20 mW of 532 nm light. In this project, two SHG configurations were explored: intracavity and external cavity.

In the intracavity configuration, a KTP crystal is placed within the laser cavity of a Nd:YVO_4-based solid-state infrared laser. This setup yielded approximately 47 mW of SHG power at a diode pump current of 1.2 A. Also the SHG-coupled pump power at 1064 nm was approximately 1 mW.

In the external cavity configuration, the output from a free-running NPRO laser at 1064 nm is frequency-doubled to 532 nm using a resonantly enhanced cavity. This cavity has a theoretical finesse of 282, a free spectral range (FSR) of 507 MHz, and a full width at half maximum (FWHM) of 1.80 MHz. To maximize the circulating power and stabilize the SHG output, the NPRO laser is locked to the cavity using the Pound-Drever-Hall (PDH) technique based on cavity transmission. With this setup, 150 μW of SHG power could be obtained for 100 mW of input power from NPRO. The target is to get atleast 20 mW of SHG power.

Keywords: intracavity SHG, external cavity SHG, diode-pumped Nd:YVO_4 lasers, NPRO lasers, PDH Locking, squeezed light.

Table of Contents

List of Figures

List of Tables

Acronyms

C-NPRO Commercial Non-Planar Ring Oscillator

BPP Beam Parameter Product

BS Beam Splitter

DPSS Diode-Pumped Solid State

EOM Electro-Optic Modulator

E-NPRO Engineered Non-Planar Ring Oscillator

FSR Free Spectral Range

FWHM Full Width at Half Maximum

IPC Input Coupler

IR Infrared

KTP Potassium Titanyl Phosphate

LDC Laser Diode Current

Nd:YAG Neodymium-doped Yttrium Aluminum Garnet

Nd:YVO_4 Neodymium-doped Yttrium Ortho Vanadate

NPRO Non-Planar Ring Oscillator

OPA Optical Parametric Amplifier

OPC Output Coupler

PDH Pound-Drever-Hall

ROC Radius of Curvature

SHG Second Harmonic Generation

SQL Squeezed Light

Chapter 1

Introduction

1.1 Relevance of the project

In 1916, Albert Einstein introduced the concept of gravitational waves (GWs) through his General Theory of Relativity, though he doubted humanity would ever build instruments sensitive enough to detect them. Nearly a century later, in 2015, the two LIGO detectors located in Hanford and Livingston, USA, made the first direct detection of gravitational waves—ripples in spacetime generated by the merger of two black holes approximately 400 million parsecs (1.3 billion light-years) from Earth [1]. Each LIGO detector is an L-shaped Michelson-type interferometer enhanced with Fabry-Pérot cavities in its 4 km-long arms. Owing to the transverse quadrupolar nature of gravitational waves, one arm contracts while the other simultaneously expands, inducing a phase shift between the laser beams travelling through the two arms. This differential change produces a strain on the order of 10^{-21} which LIGO successfully measured. Remarkably, even during this first detection, the interferometers were operating near the fundamental quantum limits of sensitivity imposed by the quantum nature of light. To push beyond these limits, quantum squeezing techniques were implemented in 2019, substantially enhancing the sensitivity and increasing the detection rate from about one astrophysical event per month to nearly one per week.

Squeezed light (SQL) generation and characterization at 1064 nm requires

1. Frequency-stabilized laser source at 1064 nm
2. Second Harmonic Generation (SHG) source at 532 nm
3. Sub-critically operated optical parametric amplifier (OPA) at 1064 nm
4. Balanced Homodyne detection for measuring the squeezing level at 1064 nm

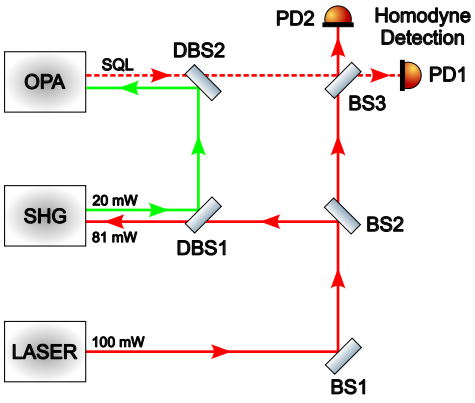

Figure 1.1: Schematic showing generation and measurement of squeezed light

The aim of this project is to develop and characterize a 532 nm SHG source for generating squeezed light at 1064 nm.

SHG can be done in three configurations:

- **Single pass:** Here the SHG conversion efficiency with continuous-wave (CW) lasers typically ranges from 10^{-5} to 10^{-2}. While this is the simplest approach, its efficiency is inherently limited. To enhance the second harmonic output, the nonlinear crystal must be placed either inside a laser cavity (intracavity SHG) or within an external resonant cavity.

- **Intracavity:** It offers the advantage of extremely high circulating powers, which can significantly boost conversion efficiency. However, a key drawback is the strong coupling between the laser dynamics and nonlinear effects, often leading to output instabilities. The detailed theory behind intracavity SHG was given by Smith [2].

- **External cavity:** It allows the use of a stable external laser (like a Non-Planar Ring Oscillator) as the pump source, with the enhancement cavity tuned independently. This configuration ensures better stability and flexibility but requires active locking between the cavity and the laser frequency for proper operation. The pump beam becomes resonant within the cavity, resulting in high intracavity power, and the generated second-harmonic power increases quadratically with the intracavity pump power [3].

1.2 Squeezed states of light

Squeezed light refers to minimum uncertainty states where quantum fluctuations are unequally distributed between conjugate quadratures. This results in noise suppression

below the standard quantum limit in one quadrature, accompanied by enhanced noise in the orthogonal quadrature, consistent with the Uncertainty relation. Such noise suppression makes squeezed states a vital resource for quantum-enhanced metrology, including applications in gravitational wave detection.

1.2.1 Quadrature operators and uncertainty

Quadrature operators $\hat{X}_1$ and $\hat{X}_2$ for the quantized form of electromagnetic field are given by [4]:

$$\hat{X}_1 = (\hat{a} + \hat{a}^\dagger), \quad \hat{X}_2 = i(\hat{a}^\dagger - \hat{a}), \tag{1.1}$$

which satisfy the commutation relation

$$[\hat{X}_1, \hat{X}_2] = 2i. \tag{1.2}$$

This leads to the uncertainty relation

$$\Delta\hat{X}_1 \, \Delta\hat{X}_2 \geq 1 \tag{1.3}$$

In a coherent state (output from a laser), the uncertainties are equal and minimal: $\Delta X_1 = \Delta X_2 = 1$. In a squeezed state, however, one quadrature (say $\hat{X}_1$) can have reduced variance ($\Delta X_1 < 1$), while the other increases accordingly such that equation (1.3) is obeyed everytime.

1.2.2 Squeezed vacuum states

A squeezed vacuum state $|0, r, \theta\rangle$ is generated by applying the squeezing operator $\hat{S}(r, \theta)$ to the vacuum state $|0\rangle$:

$$|0, r, \theta\rangle = \hat{S}(r, \theta) \, |0\rangle \, , \quad \hat{S}(r, \theta) = \exp\left[\frac{1}{2}(re^{-2i\theta}\hat{a}^2 - \frac{1}{2}re^{2i\theta}\hat{a}^{\dagger 2})\right], \tag{1.4}$$

where r is the squeezing factor and θ is the quadrature angle of the squeezing.

1.2.3 Physical realization

Squeezed light can be generated via nonlinear optical processes such as degenerate parametric down-conversion (PDC) or four-wave mixing (FWM) in $\chi^{(2)}$ or $\chi^{(3)}$ nonlinear media, respectively. In a typical degenerate optical parametric amplifier (OPA), a strong pump field at frequency 2ω interacts with a nonlinear crystal to produce correlated photon pairs at frequency ω, resulting in a squeezed vacuum state at the output.

1.3 Nd:YVO_4 laser

Neodymium-doped yttrium orthovanadate (Nd:YVO_4) is a widely used solid-state laser gain medium, valued for its high absorption efficiency, strong emission cross-section, and suitability for diode pumping. Compared to other neodymium-doped crystals such as Nd:YAG, Nd:YVO_4 offers several performance advantages in compact and high-power laser systems.

YVO_4 is a birefringent, positive uniaxial crystal with tetragonal zircon structure and excellent optical quality. It is typically doped with Nd^{3+} ions at concentrations ranging from 0.1% to 1.0%. Table 1.1 summarizes its key optical and physical properties relevant to laser applications.

Table 1.1: Key properties of Nd:YVO_4 crystal

Property	Value
Crystal structure	Tetragonal, zircon type
Emission wavelength	1064 nm (strongest), also 1342 nm, 914 nm
Emission cross-section @ 1064 nm	2.7×10^{-19} cm^2
Absorption band	808 nm (strong for diode pumping)
Absorption cross-section @ 808 nm	1.4×10^{-18} cm^2
Thermal conductivity	5.23 W/m·K (c-axis), 5.10 W/m·K (a-axis)
Refractive indices	$n_o = 1.957$, $n_e = 2.165$ @ 1064 nm
Birefringence	$\Delta n \approx 0.21$

Nd:YVO_4 supports strong linearly polarized emission due to its birefringent nature, making it well-suited for nonlinear optical processes such as frequency doubling.

1.4 Non-Planar Ring Oscillator (NPRO)

According to Koechner [5], stable single longitudinal mode operation in a laser can be reliably achieved only when certain design criteria are met:

- The use of a very short cavity, which increases the spacing between longitudinal modes such that only one mode experiences significant gain.
- Suppression of spatial hole burning caused by the standing wave pattern within the resonator.
- Unidirectional ring laser based on homogeneously broadened gain medium like Nd:YAG.

These key features are integrated in the design of a diode-pumped, monolithic NPRO illustrated in figure 1.2. The NPRO was first developed by Kane and Byer [6] in 1985.

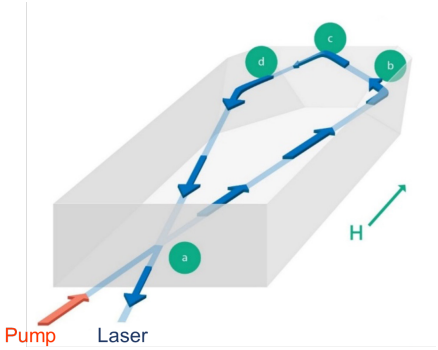

Figure 1.2: Schematic of a NPRO Laser. **Source:** `https://www.coherent.com/web-resources/white-paper/mephisto-lasers-wp`

The heart of a NPRO laser is a precisely cut monolithic crystal (typically Nd:YAG) which serves as both active medium and resonator. Most Nd:YAG NPROs are pumped using diode laser at 809 nm which is shown as a red arrow in figure (1.2). Since YAG has a non-zero Verdet constant, in the presence of a strong magnetic field, it exhibits Faraday rotation. The total internal reflections (on faces b, c, and d) act as the half-wave plates, and the output coupler (face a) acts as a partial polarizer. The Faraday rotation causes identical rotation (non-reciprocal rotation) of polarization of forward and backward travelling beams whereas the total internal reflections induce an opposite effect (reciprocal rotation). The resultant effect adds up for one beam and cancels out for the other resulting in beams with orthogonal s and p polarizations. The output coupler (face a) has varied transmission for different polarizations. The mode without polarization rotation undergoes the least loss and has the lowest threshold for oscillations. Once it starts oscillating, it clamps the gain to a lower level suppressing the other polarizations. This leads to single longitudinal mode (SLM) operation. This results in a unidirectional operation, avoiding creation of standing wave pattern and eliminating spatial hole burning.

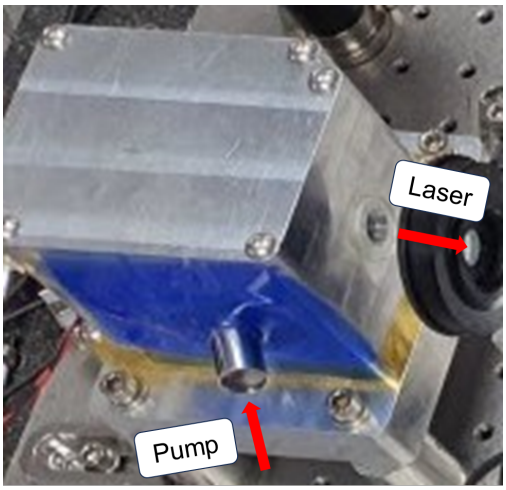

Figure 1.3: Photo of E-NPRO

The laser we are using as part of this project is an in-house developed Nd:YAG NPRO laser (shown in figure (1.3)) with the following parameters.

- Effective linewidth: $\begin{cases} \Delta\nu < 1 \text{ kHz} \\ \Delta\lambda < 3.77 \text{ pm} \end{cases}$ for 100 ms
- wavelength, λ: 1064 nm
- Crystal type: Nd:YAG
- Crystal size: 12 mm $\times$ 8 mm $\times$ 3 mm
- Temperature tunability: 3 GHz/K or 3 MHz/mK
- Voltage tunability: 4 MHz/V
- Waist: 180 μm

1.5 Fabry-Pérot cavity

A Fabry-Pérot cavity consists of two highly reflective mirrors aligned parallel to one another. The mirror on which light is incident is called input coupler (IPC) and the other mirror is called output coupler (OPC). Normally, when a beam is incident onto such a cavity, almost all of the beam will get reflected. But when the incoming beam of wavelength λ or cavity length L satisfy the condition $2L = n\lambda$, where n is an integer, the incident light will get fully transmitted through the cavity even though the mirrors are highly reflective. The condition mentioned above is nothing but the resonance condition and occurs due to interference of multiple beams inside the cavity.

The spacing in the frequency space between the longitudinal modes called free spectral range ($\Delta\nu_{FSR}$) depends on the cavity length L and is given by:

$$\Delta\nu_{FSR} = \frac{c}{2L} \tag{1.5}$$

Another important parameter is the finesse, $\mathcal{F}$ of the cavity which specifies the sharpness of the resonance peaks. For a two-mirror cavity, finesse is mathematically defined as:

$$\mathcal{F} = \frac{\pi\sqrt{r_1 r_2}}{1 - r_1 r_2} = \frac{\pi(R_1 R_2)^{\frac{1}{4}}}{1 - \sqrt{R_1 R_2}} \tag{1.6}$$

Where r_1, r_2 are the amplitude reflectivities and R_1, R_2 are the intensity reflectivities of the mirrors.

1.5.1 Estimation of finesse experimentally

- The above definition of finesse is an ideal case, but taking misalignment of the mirrors into account finesse can be defined as:

$$\mathcal{F} = \frac{\Delta\nu_{FSR}}{\Delta\nu_{FWHM}} \tag{1.7}$$

  Where $\Delta\nu_{FWHM}$ is the pass bandwidth of the cavity resonance peaks.

- There is yet another way to calculate finesse of a cavity just from the knowledge of incident and transmitted powers. The transmitted power is related to the intracavity or circulating power through the following equation:

$$P_{circ} = \frac{P_{trans}}{T_2} \tag{1.8}$$

  Where T_2 is the intensity transmission of the output coupler.

  The intracavity power and incident power are related through

$$P_{circ} \approx \frac{\mathcal{F}}{\pi} P_{inc} \tag{1.9}$$

  Where the factor $\mathcal{F}/\pi$ is called enhancement or amplification factor.

  Therefore, if the incident power is known, the finesse of the cavity can be calculated using the above equation.

An excellent reference for optical cavities is [7].

1.6 Cavity designs

This section discusses about various cavity designs like thermal lens based plane-plane cavity, advantages of folded cavity like V-cavity.

1.6.1 Thermal lens based plane-plane cavity

In conventional laser resonator design, at least one curved mirror is typically used to ensure stable resonator modes. However, in diode-pumped solid-state lasers, it is possible to realize a stable cavity using plane mirrors by exploiting the thermal lens effect within the gain medium. This approach simplifies alignment and mechanical design, particularly for compact, monolithic systems.

Origin of the Thermal Lens

When a solid-state laser crystal (e.g., Nd:YVO_4 or Nd:YAG) is optically pumped, a portion of the absorbed pump power is converted into heat due to quantum defect and non-radiative transitions. This non-uniform heat deposition creates a radial temperature gradient, which induces a refractive index profile via two mechanisms:

1. **Thermo-optic effect:** The refractive index of the crystal changes with temperature, characterized by the thermo-optic coefficient dn/dT.

2. **Thermo-elastic stress:** Thermal expansion induces mechanical stress that further modifies the refractive index via the photoelastic effect.

3. **Physical expansion effect:** Physical expansion depends on the temperature gradient due to dn/dT and physical length L of the crystal.

The combined effect results in a radially varying refractive index, typically approximated as a parabolic lens, referred to as a thermal lens.

Stability of a Plane-Plane Cavity

In a standard plane-plane (flat-flat) cavity, the absence of geometric curvature makes the resonator unstable in free space. However, if the laser crystal exhibits sufficient thermal lensing, it acts as an effective curved mirror with a focal length f_{th}, stabilizing the cavity. The cavity can be treated as a lens-like resonator where the thermal lens introduces an effective optical power. For a symmetric cavity of length L with the thermal lens at the centre, the cavity becomes stable if the following condition is satisfied:

$$0 < g_1 g_2 = \left(1 - \frac{L}{f_{\text{th}}}\right)^2 < 1, \tag{1.10}$$

where $g_1 = g_2$ due to the symmetric configuration. This criterion mirrors that of a conventional stable resonator and allows mode confinement within the cavity.

Design Considerations

When designing a thermal-lens-stabilized plane-plane cavity, key factors include:

- **Pump power dependence:** The focal length of the thermal lens varies with absorbed pump power, leading to dynamic changes in mode size and stability.

- **Crystal geometry:** The crystal length and cross-section affect heat flow and lensing strength.

- **Cooling efficiency:** Proper heat sinking and thermal management minimize aberrations and stress-induced birefringence.

- **Thermal lens aberrations:** Higher-order distortions can degrade beam quality and must be mitigated in high-power designs.

1.6.2 V-shaped cavity

A V-shaped resonator employs three mirrors arranged so that the optical axis folds through an angle at the central (folding) mirror, forming a "V" geometry. This configuration combines the simplicity of plane or curved mirrors with enhanced stability and compactness, making it popular in diode-pumped solid-state lasers and external cavity applications.

The advantages of V-shaped cavity includes

- **Compact footprint:** Folding reduces overall cavity length.
- **Enhanced stability:** curved mirror provide stronger mode control.
- **Mode size control:** The TEM_{00} beam waist can be controlled by varying the arm lengths.

1.7 Second Harmonic Generation

Second Harmonic Generation (SHG) or frequency doubling is a process where two photons, each with frequency ω interact in a nonlinear medium to create a new photon with frequency 2ω. SHG was first observed by Franken et al. in 1961 [8].

The second order nonlinear susceptibility $\chi^{(2)}$ is responsible for the SHG process and the process occurs in media that are non-centrosymmetric or media which possess no inversion symmetry as $\chi^{(2)} = 0$ for centrosymmetric media.

Under low conversion approximation:

$$\eta_{SHG} \propto l^2 d_{eff}^2 I_\omega \operatorname{sinc}^2(\Delta k l/2) \tag{1.11}$$

Where l is the crystal length, d_{eff} is the effective nonlinearity, I_ω is the intensity of the fundamental wave, and Δk is the phase mismatch.

1.7.1 Phase Matching

Efficient SHG requires that the generated second harmonic wave (2ω) remains in phase with the driving nonlinear polarization. If the fundamental and second harmonic waves propagate at different phase velocities, destructive interference occurs, reducing the conversion efficiency. Phase matching is actually the momentum conservation condition of the SHG process where the phase velocities of fundamental and second harmonic waves are equal. Good phase matching results in higher conversion efficiency.

The condition for perfect phase matching is:

$$\Delta k = k_{2\omega} - 2k_{\omega} = 0 \tag{1.12}$$

where:

- $k_{2\omega}$ is the wavevector of the second harmonic wave,
- k_{ω} is the wavevector of the fundamental wave.

Since $k = \omega n(\omega)/c$, this condition implies:

$$n(2\omega) = n(\omega) \tag{1.13}$$

The above condition is only possible in birefringent materials.

Type I and Type II Phase Matching

- **Type I:** Both fundamental photons have the same polarization (ordinary), and the second harmonic is extraordinary.

$$\left.\begin{array}{c} o + o \rightarrow e \\ n_e(2\omega) = n_o(\omega) \end{array}\right\} \quad \text{(negative uniaxial)} \tag{1.14}$$

$$\left.\begin{array}{c} e + e \rightarrow o \\ n_o(2\omega) = n_e(\omega) \end{array}\right\} \quad \text{(positive uniaxial)} \tag{1.15}$$

- **Type II:** Fundamental photons have orthogonal polarizations.

$$\left.\begin{array}{c} o + e \rightarrow e \\ n_e(\omega) + n_o(\omega) = 2n_e(2\omega) \end{array}\right\} \quad \text{(negative biaxial)} \tag{1.16}$$

$$\left.\begin{array}{c} o + e \rightarrow o \\ n_e(\omega) + n_o(\omega) = 2n_o(2\omega) \end{array}\right\} \quad \text{(positive biaxial)} \tag{1.17}$$

1.8 Acceptance Bandwidths

The parameters affecting Δk can be expressed as:

$$\Delta k = \beta_{\theta}\delta\theta + \beta_T \delta T + \beta_{\lambda}\delta\lambda \tag{1.18}$$

- $\delta\theta$ represents angular deviation (e.g., beam divergence, tilt, or crystal miscut)
- δT represents deviation from the phase-matching temperature.

- $\delta\lambda$ is the deviation in laser wavelength or spectral bandwidth.

- β_θ, β_T, and β_λ are corresponding phase mismatch sensitivity coefficients.

The acceptance bandwidths are inversely related to the corresponding sensitivity coefficients.

1.8.1 Temperature-controlled mount for KTP

Our KTP crystal is one-side HR-coated with a length of 0.7 mm. Therefore the effective length is 1.4 cm. The temperature acceptance is specified as 24 °C-cm. Hence, the temperature acceptance bandwidth is $24/1.4 \approx 17$ °C. Assuming the type-II phase matching temperature is 25 °C, this implies that increasing the crystal temperature from 25 °C to 33.5 °C, or decreasing it to 16.5 °C, will reduce the SHG conversion efficiency by half.

To maintain the KTP temperature close to the phase-matching point, a custom mount incorporating an AD590 temperature sensor was developed (see figure (1.4a)). The surface in contact with the KTP crystal is made of gold-coated copper to ensure good thermal conductivity and uniform temperature distribution.

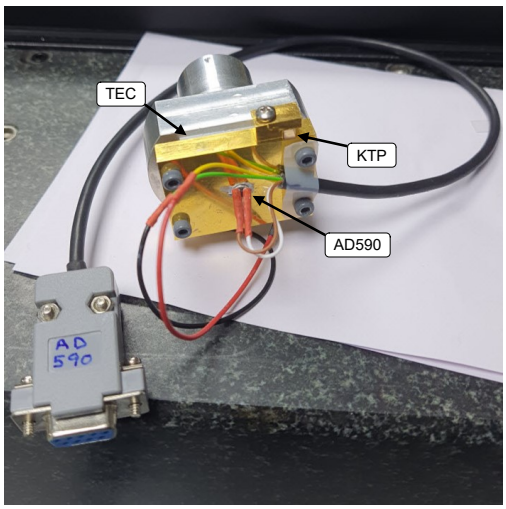

(a) KTP mount

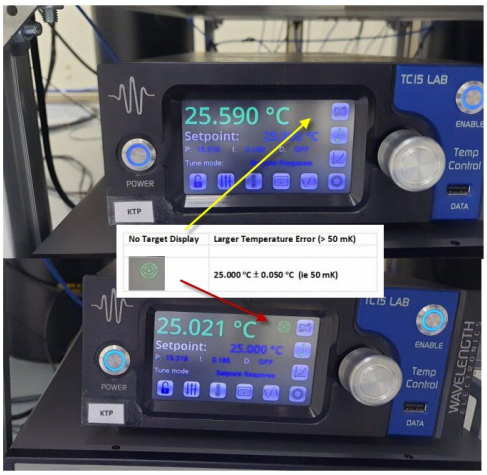

(b) Temperature controller

Figure 1.4: KTP mount and temperature controller

The purpose of this mount is to maintain the KTP crystal at a temperature close to 25 °C, with fluctuations limited to within 50 mK. The temperature is regulated using a TC15 Lab Precision temperature controller. When the actual temperature is within 50 mK of the setpoint, a green target icon appears on the controller display, as shown in Figure 1.4b.

1.9 Frequency locking

A free running laser can be locked to one of the resonance peak of a stable reference cavity resulting in reduction of linewidth of laser and frequency noise. On the other hand, a cavity can be locked to a laser and this will result in enhanced circulating power inside the locked cavity.

There are various techniques for locking a laser to a reference cavity or a slave cavity to a master oscillator.

1.9.1 Dither locking

If we want to lock a laser to a cavity or vice-versa just by looking at the transmitted intensity through the cavity, it would be almost impossible to achieve as the transmitted intensity decreases on either side of resonance peak but this is not the case with it's derivative. The derivative is anti-symmetric about the centre of the resonance peak.

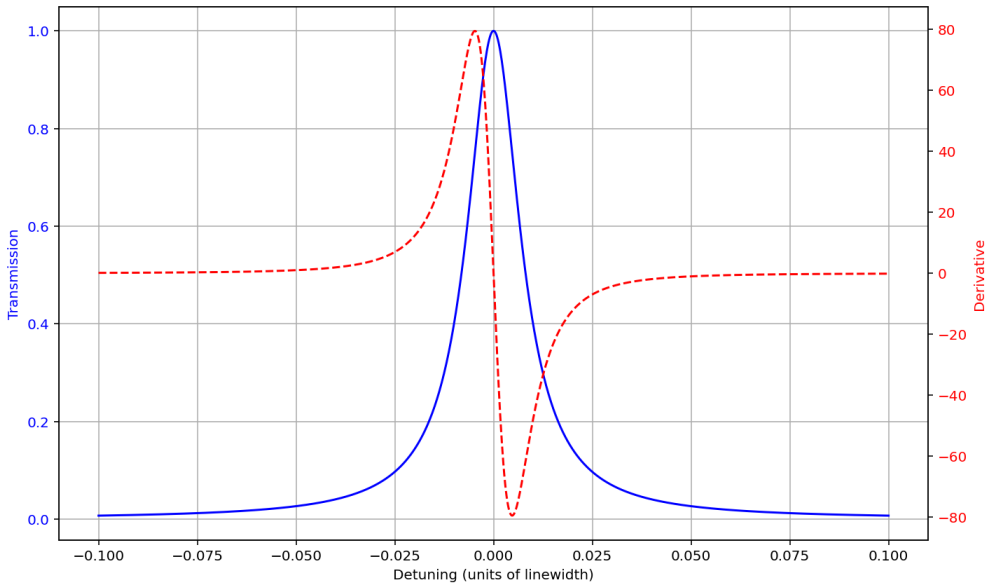

Figure 1.5: Cavity transmission and its derivative

So if a known change in the laser frequency is induced through modulation and we look for the corresponding change in intensity, the information about derivative of intensity w.r.t frequency can be obtained. In Dither locking, the laser frequency is dithered with an amplitude of about one-tenth of the pass band-width of the cavity. The transmitted signal through the cavity is used for error signal generation which is then fed back to the cavity for locking. In order to lock the laser frequency to the centre of the resonance peak, we have to know how output intensity varies with change in the laser frequency or mathematically, the derivative of intensity w.r.t. laser frequency. This is

done by modulating the laser frequency at a particular frequency and mixing the transmitted signal through the cavity with that from the local oscillator. The resulting signal after passing through low pass filter is the derivative of the intensity w.r.t. the laser frequency. This signal is then fed to the PI controller which converts it into appropriate voltage values and moves the PZT based on the position of the laser frequency w.r.t. the centre of the resonance peak.

Similarly, if we want to lock the cavity to the laser frequency, the cavity length needs to be modulated and the feedback loop is connected to the PZT attached to one of the cavity mirrors. Modulating cavity length will result in modulation of transmitted intensity through the cavity which will provide information about first derivative of intensity w.r.t laser frequency. Here the cavity length will get adjusted based on the laser frequency.

Let's assume the laser frequency is centred at ω_0 which is dithered sinusoidally at frequency Ω with a scan of $\Delta\omega$. The modulated beam after transmission through the cavity is incident on a photodiode which creates a voltage oscillating proportional to the frequency dithered beam given by (using the definition of derivatives):

$$V(\omega) = V(\omega_0 + \Delta\omega\cos\Omega t) = V(\omega_0) + \frac{dV(\omega_0)}{d\omega}\Delta\omega\cos\Omega t + ...$$

Since modulation frequency Ω is high (in kHz), the higher order terms of Ω can be neglected.

$$V(\omega_0 + \Delta\omega\cos\Omega t) \approx V(\omega_0) + \frac{dV(\omega_0)}{d\omega}\Delta\omega\cos\Omega t \tag{1.19}$$

To generate the error signal $\varepsilon(t)$, the photodiode output ($V(\omega_0 + \Delta\omega\cos\Omega t)$) is mixed with the original modulation signal ($\cos\Omega t$) to form $\varepsilon'(t)$ which is then passed through a low-pass filter.

$$\begin{aligned}
\varepsilon'(t) &= V(\omega_0 + \Delta\omega\cos\Omega t)\cos\Omega t \qquad (1.20)\\
\varepsilon'(t) &\approx \left[V(\omega_0) + \frac{dV(\omega_0)}{d\omega}\Delta\omega\cos\Omega t\right]\cos\Omega t\\
\varepsilon'(t) &= V(\omega_0)\cos\Omega t + \frac{dV(\omega_0)}{d\omega}\Delta\omega\cos^2\Omega t
\end{aligned}$$

Using the trigonometric identity

$$\cos^2\Omega t = \frac{1+\cos 2\Omega t}{2}$$

$$\varepsilon'(t) = V(\omega_0)\cos\Omega t + \frac{dV(\omega_0)}{d\omega}\Delta\omega + \frac{dV(\omega_0)}{d\omega}\Delta\omega\cos 2\Omega t \tag{1.21}$$

This signal is then passed through a low pass filter which blocks the high frequency components (Ω, 2Ω, ...) and only allows the DC term to pass, resulting in the final expression for the error signal

$$\varepsilon(t) = \frac{dV(\omega_0)}{d\omega}\Delta\omega \tag{1.22}$$

The final signal is the dither error signal which has the required property of correction at the resonance, i.e., $\varepsilon = 0$ and $\frac{d\varepsilon}{d\omega} \neq 0$ (i.e., anti-symmetric about the resonance).

1.9.2 Pound-Drever-Hall locking

The Pound-Drever-Hall or in short, PDH technique was first demonstrated for microwaves by R. V. Pound in the 1940s. The concept was applied to the optical regime by Ronald Drever [9] in the 1980s and implemented by Jan Hall's group at JILA.

Reflection-based PDH

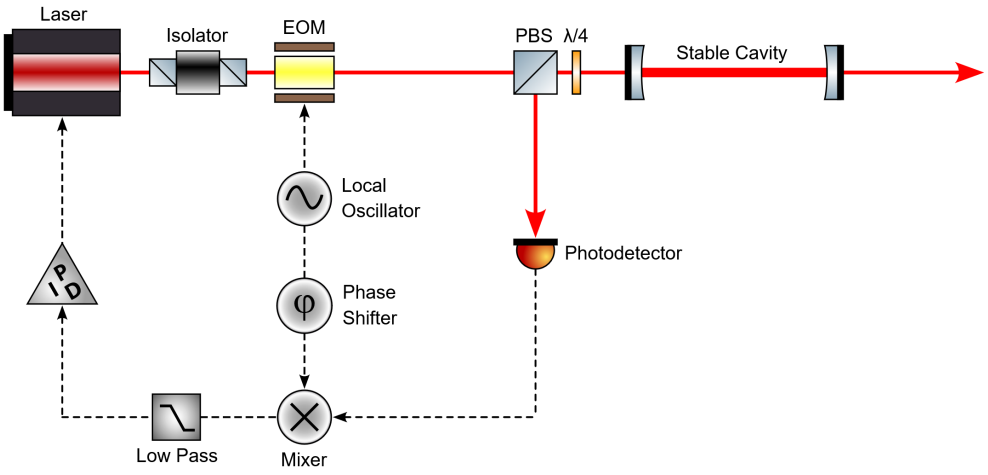

Figure 1.6: Schematic of a basic PDH lock setup

In PDH technique, the phase of the laser beam is modulated with a frequency greater (4 to 5 times) than the pass bandwidth of the cavity using an EOM which results in two sidebands about the resonance peak. When this phase modulated beam is incident on the cavity, the sidebands being outside the pass bandwidth, always get reflected but the nature of carrier signal depends on the relative frequency difference between the laser frequency and the nearest resonance peak. When this difference is zero, the entire carrier signal gets transmitted through the cavity. But for non-zero frequency differences, there is some component of reflected beam which can interfere with the

sidebands to produce a beat signal and this beat signal has the information about the phase of the reflected beam. Since phase is anti-symmetric unlike reflected intensity, we can generate a bipolar error signal by mixing this beat signal with the modulation signal from local oscillator. An intuitive and comprehensive treatment of the PDH technique is given by Black [10, 11] and Nickerson [12].

The electric field of the laser is given by

$$E_{laser} = E_0 e^{i\omega t} \tag{1.23}$$

The beam undergoes phase modulation via the EOM, operating at a frequency $\Omega/2\pi$ and a modulation index β. Therefore beam passing through the EOM or the beam which is incident onto the cavity can be written as

$$E_{inc} = E_0 e^{i(\omega t + \beta \sin \Omega t)} \tag{1.24}$$

Using the relation

$$e^{iz\sin\theta} = \sum_{n=-\infty}^{\infty} J_n(z) e^{in\theta} \tag{1.25}$$

Where J_n is the Bessel function of the first kind with order n.

Equation (1.24) can be written as

$$E_{inc} = E_0 e^{i\omega t}(J_0(\beta) + J_1(\beta)e^{i\Omega t} + J_2(\beta)e^{2i\Omega t} + ...) \tag{1.26}$$

$$E_{inc} \approx E_0 e^{i\omega t}(J_0(\beta) + 2iJ_1(\beta)\sin\Omega t) \tag{1.27}$$

$$E_{inc} = E_0 e^{i\omega t}\left(J_0(\beta) + 2iJ_1(\beta)\frac{(e^{i\Omega t} - e^{-i\Omega t})}{2i}\right)$$

$$E_{inc} = E_0\left(J_0(\beta) + J_1(\beta)e^{i(\omega+\Omega)t} - J_1(\beta)e^{i(\omega-\Omega)t}\right) \tag{1.28}$$

Equation (1.28) tells that due to phase modulation, two sidebands, one with frequency $(\omega+\Omega)/2\pi$ and other with frequency $(\omega-\Omega)/2\pi$ are induced on either sides of the carrier wave with frequency $\omega/2\pi$. Therefore the incident beam now has to be treated as three different beams (a carrier with two sidebands).

To calculate the field of the beam reflected from the cavity, each beam has to be multiplied by the reflection coefficient (F) at the appropriate frequency. Therefore, the reflected field

$$E_{ref} = E_0\left(F(\omega)J_0(\beta) + F(\omega+\Omega)J_1(\beta)e^{i(\omega+\Omega)t} - F(\omega-\Omega)J_1(\beta)e^{i(\omega-\Omega)t}\right) \tag{1.29}$$

But we measure power not electric field with a photodetector.

$$P_{ref} = \left|E_{ref}\right|^2 = E^*_{ref}E_{ref}$$

On solving,

$$\begin{aligned} P_{ref} &= P_c|F(\omega)|^2 + P_s[|F(\omega+\Omega)|^2 + |F(\omega-\Omega)|^2] \\ &+ 2\sqrt{P_c P_s} Re[F(\omega)F^*(\omega+\Omega) - F^*(\omega)F(\omega-\Omega)]\cos\Omega t \\ &+ 2\sqrt{P_c P_s} Im[F(\omega)F^*(\omega+\Omega) - F^*(\omega)F(\omega-\Omega)]\sin\Omega t \\ &+ (2\Omega\, terms) \end{aligned} \tag{1.30}$$

The interference between carrier and sidebands gives rise to The Ω terms whereas the 2Ω terms arise from interference between the sidebands. Our terms of interest are the two terms that oscillate at the modulation frequency Ω. This is because they sample the phase of the reflected beam. These are the sine and cosine terms in equation (1.30).

To extract the phase information, it is necessary to isolate one of the oscillating components of the detected signal. At high modulation frequencies, the term involving $\sin\Omega t$ multiplied by the imaginary part of $F(\omega)$ becomes dominant. This term is directly proportional to the original modulation signal applied to the EOM, allowing it to be extracted using a mixer. A mixer is an electronic device that multiplies two input signals; in this case, combining the photodetector output, $P_{\text{inc}} \propto \sin\Omega t$, with a reference signal $\sin\Omega t$ from a local oscillator yields a sum of a DC term and an oscillating $\cos\Omega t$ component:

$$\sin\Omega t \cdot \sin\Omega t = \frac{1}{2}(1 - \cos 2\Omega t)$$

By applying a low-pass filter to remove the high-frequency term $\cos 2\Omega t$, the remaining DC component is isolated. This forms the PDH error signal, which is proportional to the imaginary part of the cavity response and can be used for laser frequency stabilization.

$$\varepsilon = 2\sqrt{P_c P_s}\,\mathrm{Im}\,[F(\omega)F^*(\omega+\Omega) - F^*(\omega)F(\omega-\Omega)] \tag{1.31}$$

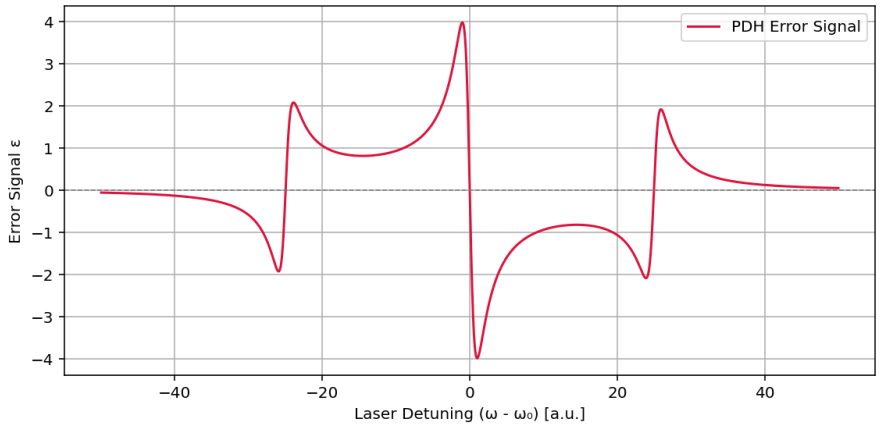

Figure 1.7: Plot of the reflection PDH error signal

Transmission-based PDH

Just like dither locking, in transmission PDH locking, the transmitted beam through the cavity is used to generate error signal. This is particularly useful when dealing with low finesse cavities where the reflection-based PDH cannot be implemented. The error signal generated with this technique has a very identical form to that of dither. Since the sidebands will get transmitted, there will be no secondary error signals around the centre which is present in reflection-based PDH.

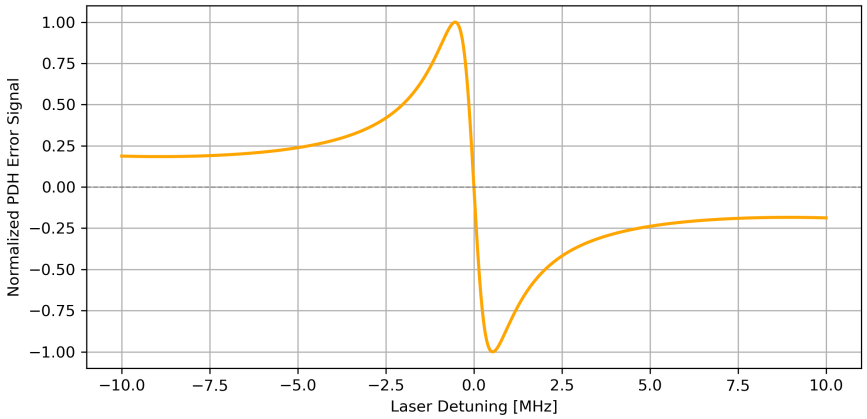

Figure 1.8: Plot of the transmission PDH error signal

1.9.3 A comparison between Dither and PDH

Table 1.2: Comparison between Pound-Drever-Hall (PDH) and Dither Locking Techniques

Feature	**Pound-Drever-Hall (PDH)**	**Dither Locking**
Modulation Type	High-frequency phase modulation (typically RF)	Low-frequency amplitude or phase modulation (typically a few kHz)
Error Signal Generation	Based on interference between carrier and reflected sidebands from the cavity	Based on amplitude response of the transmitted or reflected signal to dither
Signal-to-Noise Ratio (SNR)	High; ideal for narrow linewidth and high-finesse cavities	Lower SNR, especially for narrow features or low-finesse systems
Complexity	Requires RF electronics, mixers, and careful phase control	Simpler electronics; can be implemented with basic lock-in detection
Lock Quality	High precision, very low residual frequency noise	Moderate, depending on dither amplitude and detection sensitivity

1.10 Proposed plan of work

The proposed plan involves developing the SHG source using two approaches:

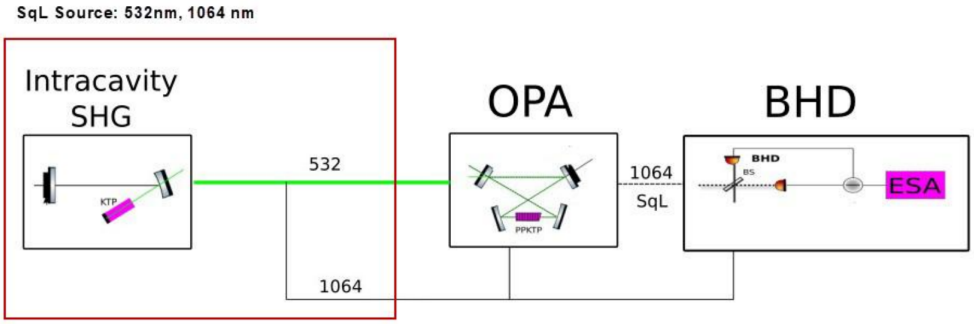

Figure 1.9: Schematic of intracavity-based squeezed light source setup

- **Intracavity**: Figure (1.9) depicts the topology for squeezed light generation using an intracavity frequency-doubled SHG source at 532 nm. The section marked in red box highlights my project component which involves generating SHG using a diode-end-pumped Nd:YVO_4 laser and a KTP crystal as the intracavity frequency doubler.

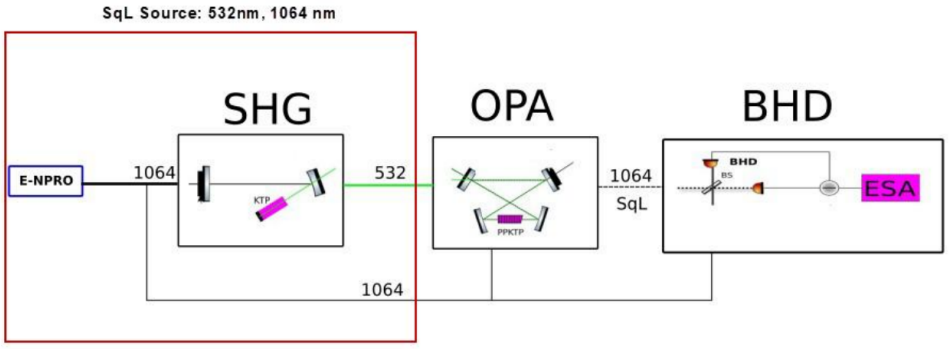

Figure 1.10: Schematic of external cavity-based squeezed light source setup

- **External cavity**: Figure (1.10) illustrates the topology for squeezed light generation using an external cavity frequency-doubled SHG source at 532 nm. The section highlighted in red box represents my project scope which involves generating SHG at 532 nm using a NPRO laser as the pump source and a KTP crystal for intracavity doubling. A PDH-based frequency locking technique will be employed to enhance the SHG power.

Chapter 2

Preliminary set of experiments

The work presented in this chapter was carried out to gain hands-on experience in building, operating, and characterizing various laser systems and their output beams. The laser systems studied include a diode laser and a Nd:YVO_4-based infrared laser. Key characterizations such as *L-I* curves, slope efficiency studies, and beam quality (M^2) measurements were performed. Several of these experiments also proved beneficial during the later stages of the project.

2.1 Diode laser

The diode laser used here is a edge-emitting type semiconductor laser from Coherent. The power supply is an in-house developed Laser Diode (LD) current and temperature controller. The emitted wavelength of 809 nm is delivered into a 2x telescope through an optical fiber. The telescope consisting of two convex lenses, focuses the beam with a beam waist of 100 μm. This laser will be further used to end-pump a $NdYVO_4$ crystal to emit 1064 nm.

2.1.1 *L-I* characteristics

The output laser power (P_{LD}) and the laser diode current (I_{LD}) are related as

$$P_{LD} = SF(I_{LD} - I_{th}) \tag{2.1}$$

Where SF is the slope factor and I_{th} is the threshold current.

The diode current was varied and the laser output at 809 nm was measured using an Ophir 3A power meter. Then a linear fit was done using equation (2.1) to find slope factor ($SF = 931.48 \pm 9.53$ mW/A) and threshold diode current ($I_{th} = 0.281 \pm 0.001$ A).

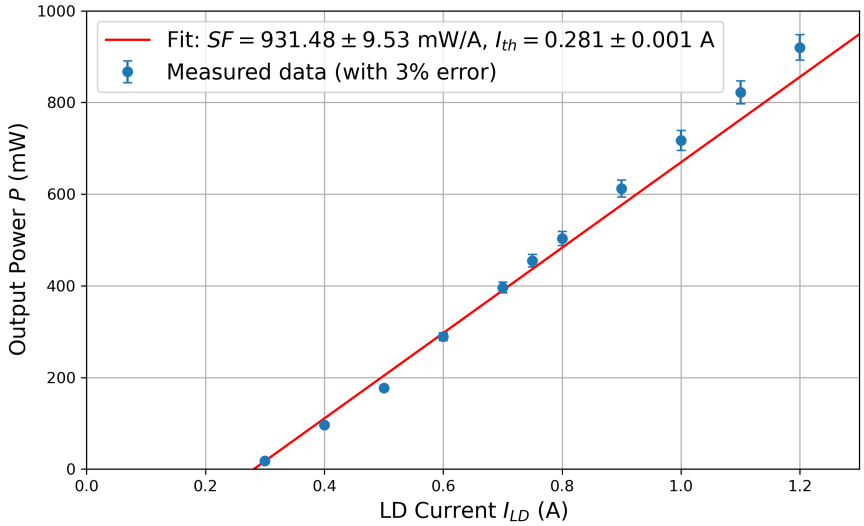

Figure 2.1: *L-I* characteristics plot for diode laser

2.2 Diode-pumped Nd:YVO_4 based IR laser

This laser was constructed using a 2 at-%-doped 1 mm long Nd:YVO_4 crystal, end-pumped with the 809 nm diode laser. The speciality of Nd:YVO_4 is that it has an emission cross section which is five times than that of Nd:YAG and exhibit a strong absorption at 809 nm due to which very short length crystals can be used. The 809 nm beam coming out of the 2x telescope is focussed inside the Nd:YVO_4 crystal through the face which is HR @ 1064 nm and HT @ 809 nm. Then a output coupling mirror of T = 5% @ 1064 nm was placed at a distance of about 10-15 mm to form a two-mirror cavity that was resonant for 1064 nm.

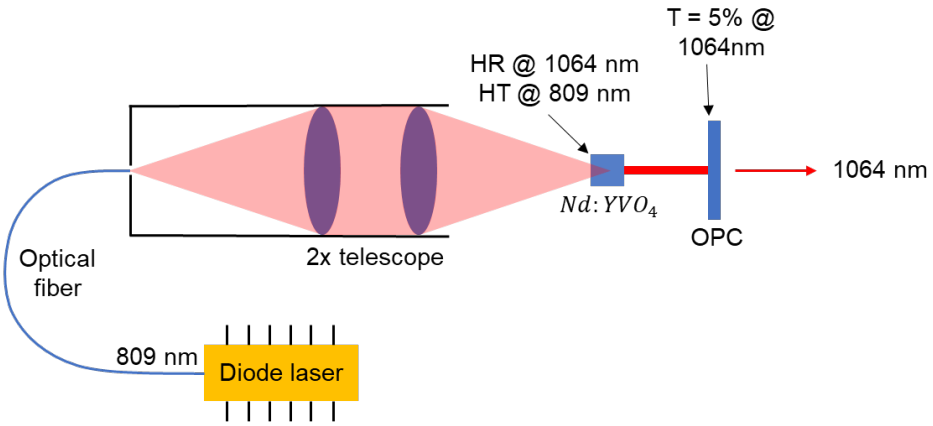

Figure 2.2: Schematic of the setup

The heat from the focused pump beam inside Nd:YVO_4 creates thermal gradients which in turns create gradients in refractive index due to which the crystal behaves like a lens. This effect is called thermal lensing. This internal lens generated within

the active medium transforms the plane-plane cavity into a curved mirror cavity and therefore brings the unstable cavity into geometrical stability.

2.2.1 *L-I* characteristics

The output IR power (P_{IR}) and the laser diode current (I_{LD}) are related as

$$P_{IR} = SF(I_{LD} - I_{th}) \tag{2.2}$$

Where SF is the slope factor and I_{th} is the threshold current.

The diode current was varied and the laser output at 1064 nm was measured using an Ophir 3A power meter. Then a linear fit was done using equation (2.2) to find slope factor (SF = 310.73 $\pm$ 3.89 mW/A) and threshold diode current (I_{th} = 0.469 $\pm$ 0.001 A).

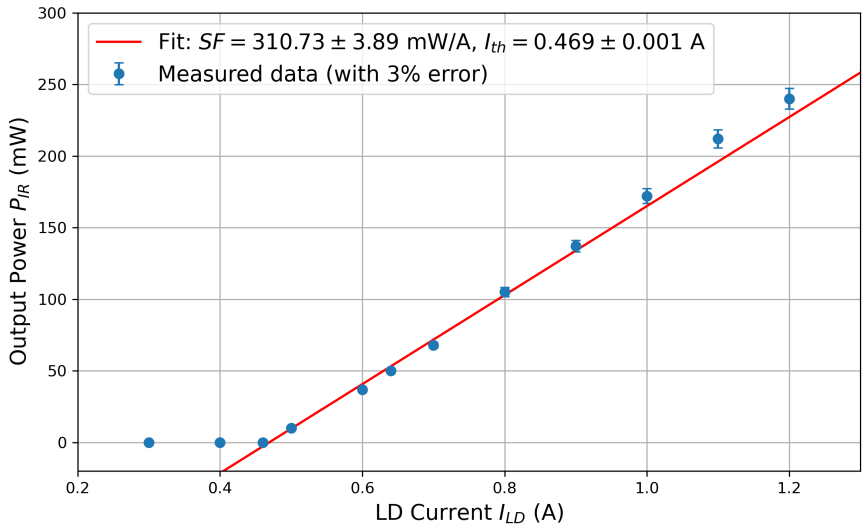

Figure 2.3: *L-I* characteristics plot for diode-pumped Nd:YVO_4 laser

2.2.2 Slope Efficiency

The output laser power at 1064 nm (P_{IR}) and the input pump power at 809 nm (P_{LD}) are related as

$$P_{IR} = SE(P_{LD} - P_{th}) \tag{2.3}$$

Where SE is the slope efficiency and P_{th} is the threshold pump power.

The output powers of the IR laser and the diode laser were measured and plotted against the laser diode current, and a linear fit based on equation (2.3) was done to estimate the slope efficiency (SE = 0.316 $\pm$ 0.006) and the threshold pump power (P_{th} = 166.9 $\pm$ 9.2 mW).

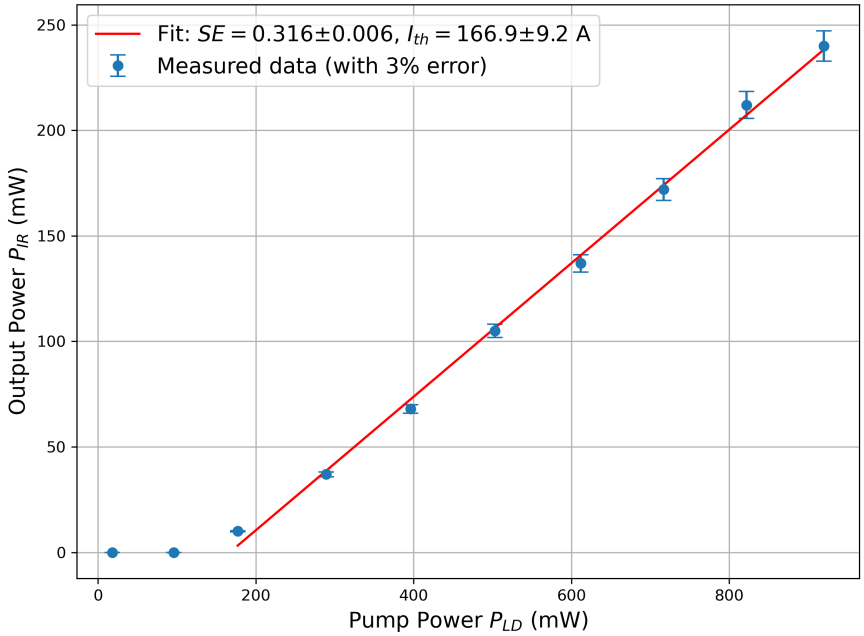

Figure 2.4: Slope efficiency plot for diode-pumped Nd:YVO_4 laser

2.2.3 M^2 measurement

The beam quality factor, represented as M^2 is defined as the ratio of beam parameter product (BPP = $\omega\theta$) of the beam to that of an ideal Gaussian beam and is mathematically given by the following equation

$$M^2 = \frac{\omega\theta}{\omega_0\theta_0} \tag{2.4}$$

Where θ is the half-angle beam divergence at the far field and ω is the beam waist. The parameters with subscript "0" are for the ideal Gaussian beam.

An ideal Gaussian beam has lowest BPP value of λ/π and $M^2 = 1$. For real beams, M^2 is always greater than 1. The closer the value is to 1, the higher will be the beam quality. In physical sense, the M^2 parameter tells about two things.

1. How well a collimated beam focuses.

2. How well a divergent beam is collimated.

There are many methods to the measure M^2 parameter. The method used here is the knife-edge method in which a sharp blade attached to a X-Y stage cuts the beam at locations (orthogonal to the beam propagation direction) where power reduces to 90% and 10% of the total power. Lets assume these two locations be $X_{90\%}$ $X_{10\%}$ respectively. The beam radius is then calculated using the equation

$$\Delta\omega = 0.7805(X_{90\%} - X_{10\%}) \tag{2.5}$$

The procedure is repeated at different locations about the beam waist location and a nonlinear fit is done using the following equation (2.6).

$$\omega(z) = \omega_0 \sqrt{1 + \left(\frac{M^2 \lambda (z - z_0)}{\pi \omega_0^2} \right)^2} \tag{2.6}$$

Where ω_0 is the beam waist, z_0 is the waist location, and λ is the wavelength of the beam.

The M^2 of the diode-pumped IR laser was found to be 1.12 ± 0.02.

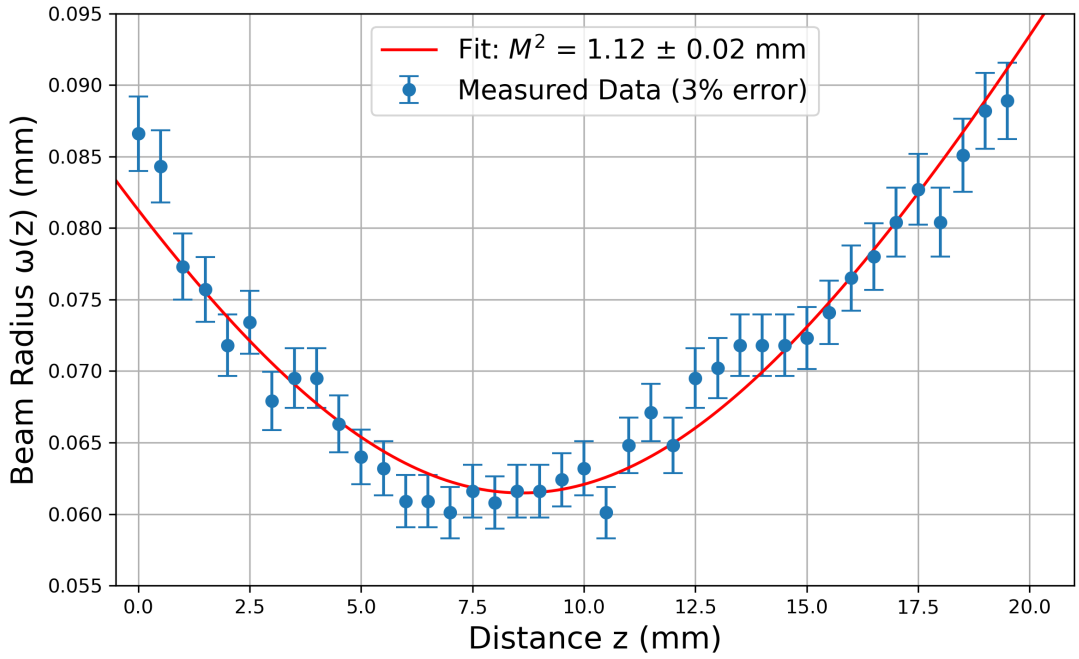

Figure 2.5: M^2 for diode-pumped IR laser

2.3 PDH versus Dither Locking study

Our paper titled, "Investigation of PDH and Dither locking techniques for an in-house developed NPRO laser with a reference cavity" was accepted for poster presentation at the National Laser Symposium - 33 which was held during 6 - 7 March 2025 at Medicaps University, Indore.

In the first part, the NPRO laser was locked to a confocal reference cavity with finesse 230 and pass-bandwidth 6.5 MHz using reflection PDH technique. Here the phase of the NPRO laser was modulated at 25 MHz to generate sidebands outside the cavity pass-bandwidth and the reflected signal from the cavity was used to generate error signal. The stability of the transmitted power was 0.40%.

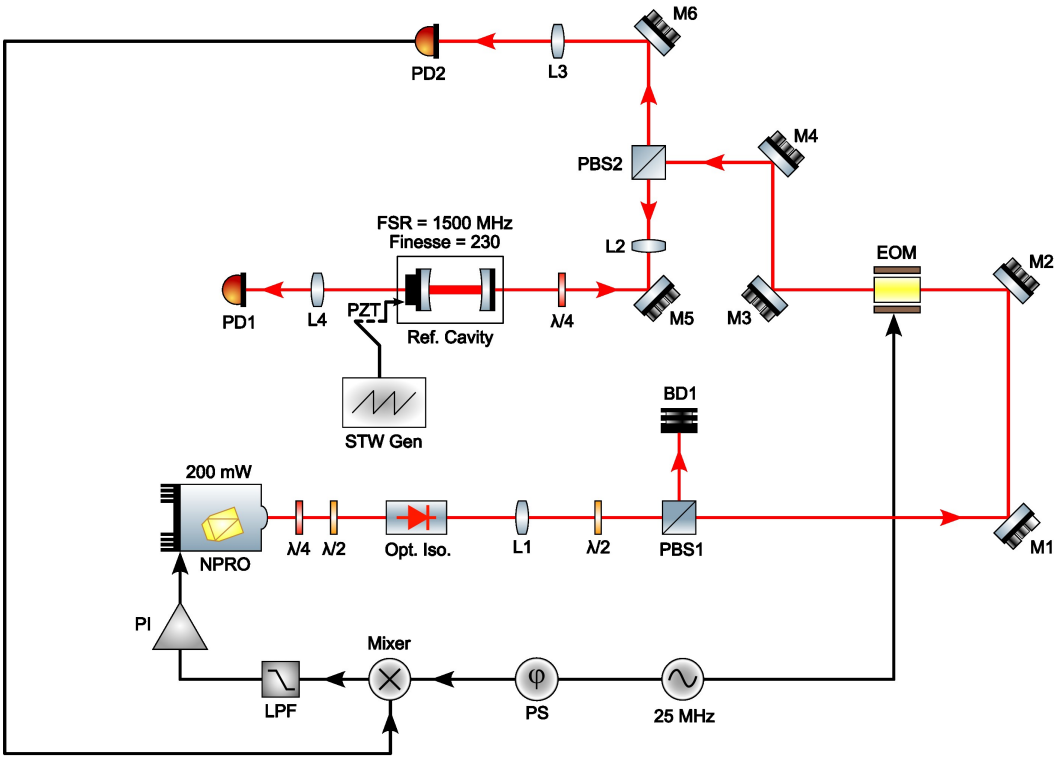

Figure 2.6: PDH locking setup

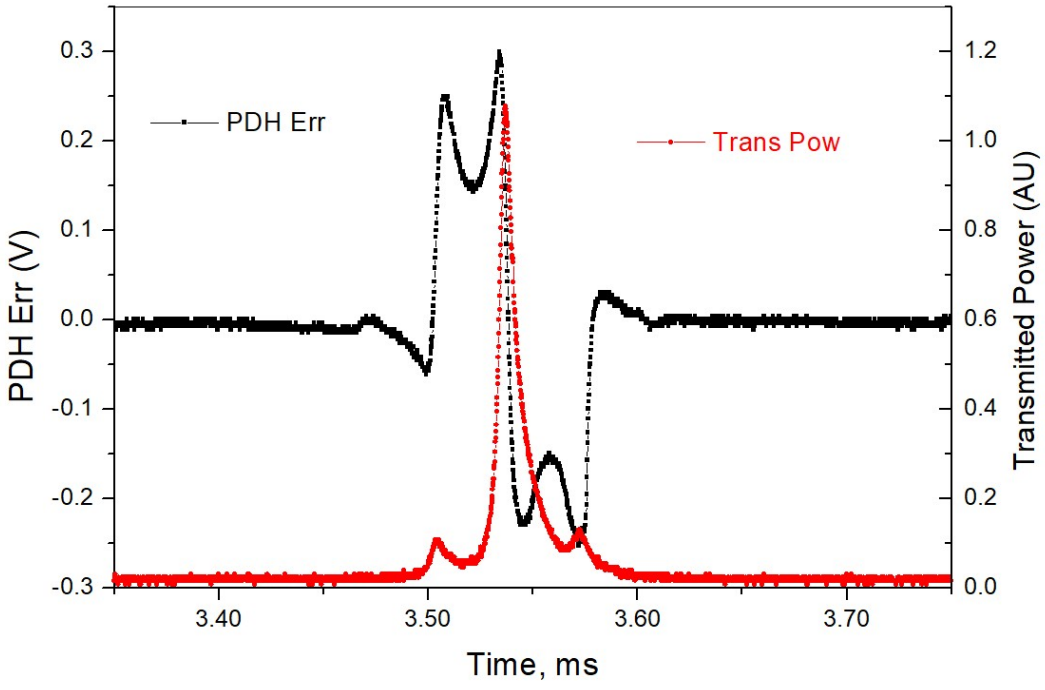

Figure 2.7: PDH error signal

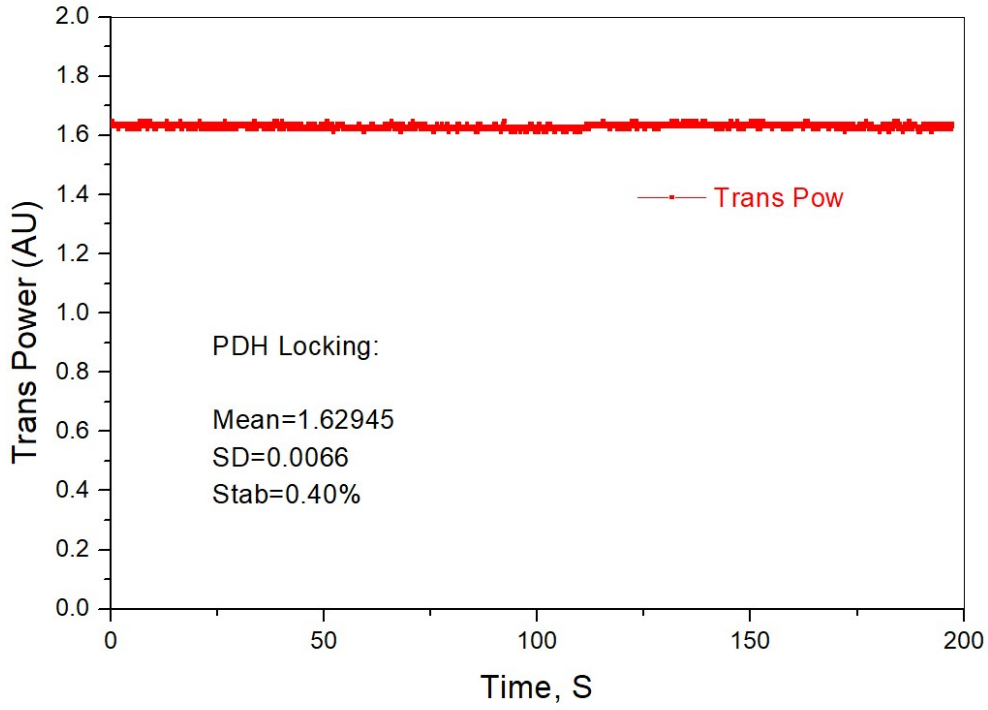

Figure 2.8: Cavity transmitted power

In the second part, a plane-plane reference cavity with finesse 15 and pass-bandwidth 213 MHz was locked to the NPRO using Dither technique. The laser frequency was modulated at 4 MHz using a local oscillator. The error signal generation was done using signal mixing of local oscillator and transmitted signal. The local oscillator, mixer, low-pass filter, and PI controller were all part of the Moku Lab lock-in amplifier. The stability of the transmitted power was 0.48%.

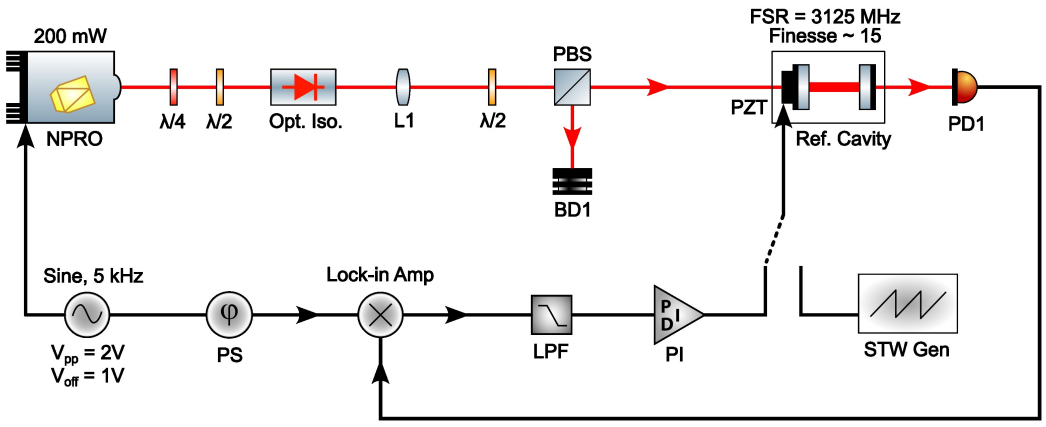

Figure 2.9: Dither locking setup

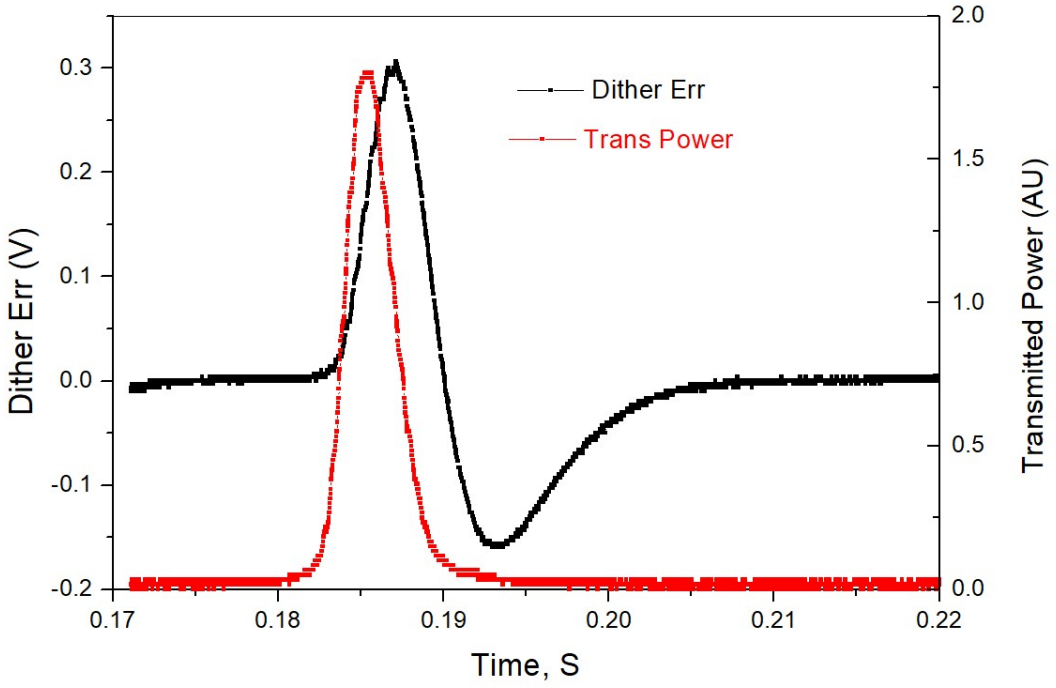

Figure 2.10: Dither error signal

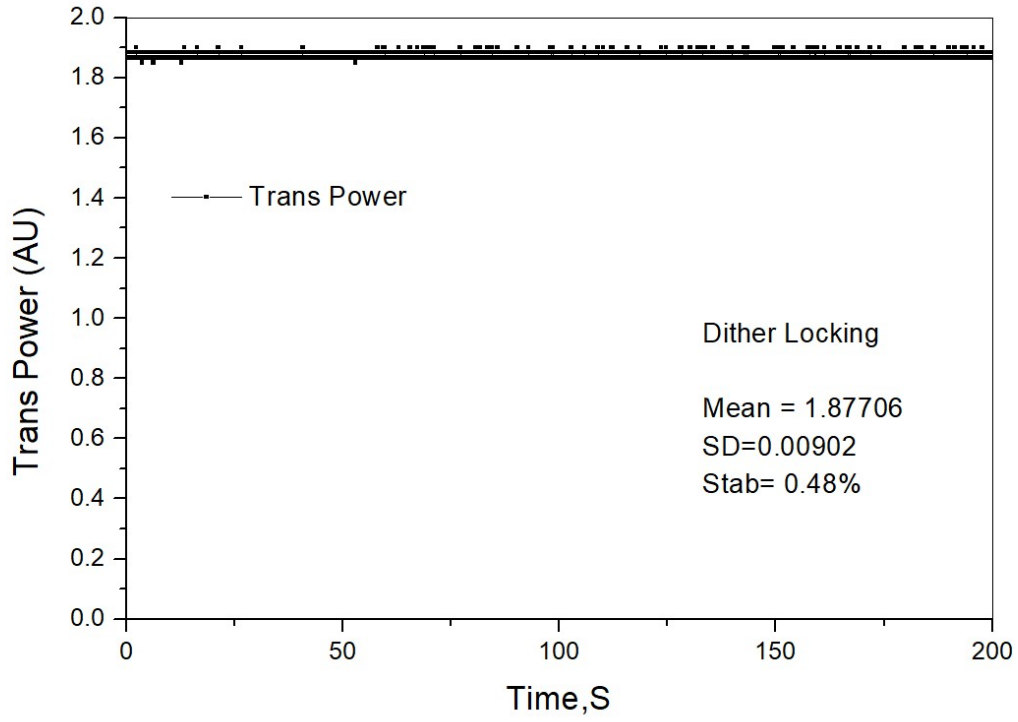

Figure 2.11: Cavity transmission

Chapter 3

Intracavity SHG source at 532 nm

This chapter presents the intracavity SHG source using Nd:YVO_4, covering its design using reZonator software and subsequent performance studies.

3.1 Estimation of optimum beam waist inside KTP

For estimating the optimal spot size for a given crystal of length L, the following condition must be satisfied:

$$L \approx z_R = \frac{\pi \omega_0^2 n}{\lambda} \tag{3.1}$$

Where z_R is the Rayleigh range, n is the refractive index of the crystal, and λ is the wavelength of light used.

For effective L = 14 mm, λ = 1064 nm, and n = 1.75, the optimum spot comes out to be 37 μm.

3.2 V-cavity design and simulation

ReZonator v2.0.14 rc1 [13] was used to simulate the V-cavity. Figure (3.1) shows the actual diagram of the V-cavity for intracavity SHG. The objective of this simulation was to find the values of d1 and d2 such that the beam waist inside KTP is close to the optimum value of 37 μm.

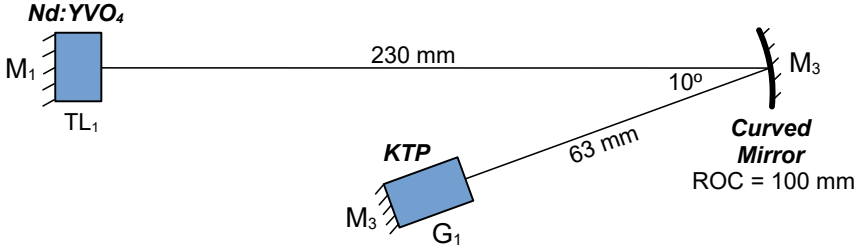

Figure 3.1: Schematic of the V-cavity used for intracavity SHG

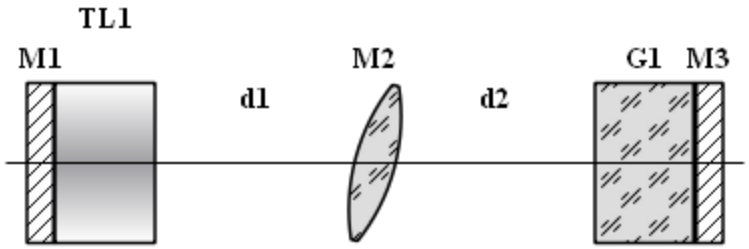

Figure 3.2: Equivalent model for the V-cavity used for intracavity SHG

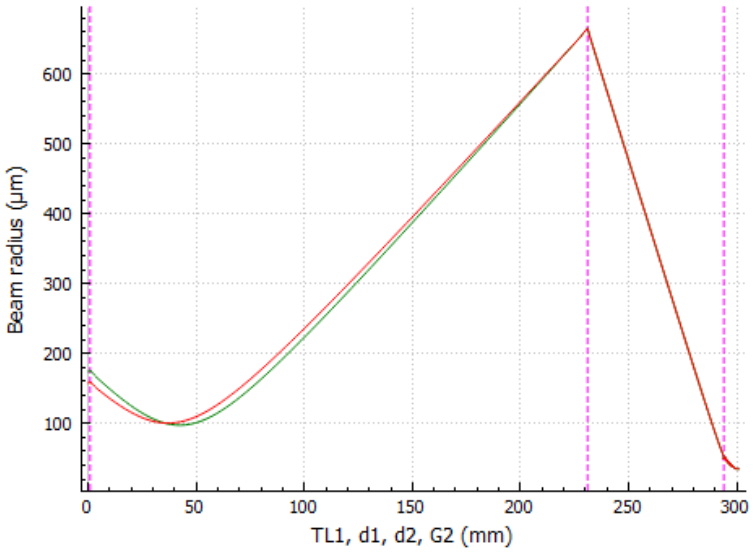

Figure 3.3: Cavity eigenmode of the V-cavity used for intracavity SHG

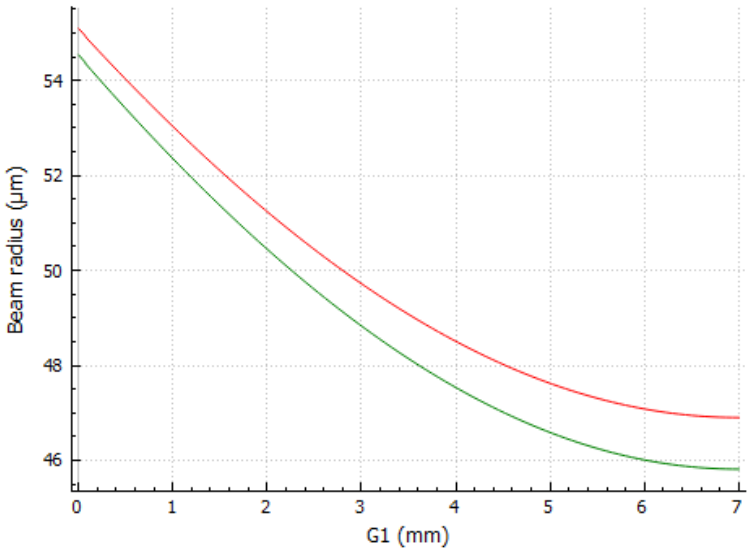

Figure 3.4: Beam waist inside KTP of the V-cavity used for intracavity SHG

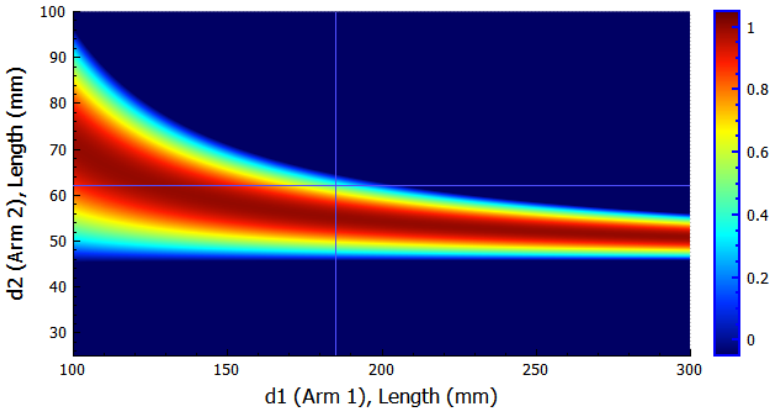

Figure 3.5: Stability plot of the V-cavity used for intracavity SHG

3.3 Experimental Setup

This is a V-shaped intracavity doubled green laser. Here a diode laser end pumps a Nd:YVO_4 crystal at 809 nm resulting in laser emission at 1064 nm. The 1064 nm beam is frequency doubled using a KTP crystal present inside the laser cavity.

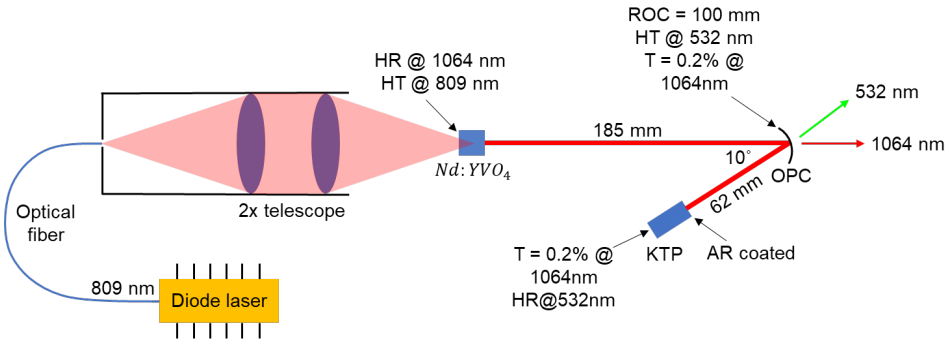

Figure 3.6: Schematic of the intracavity SHG setup

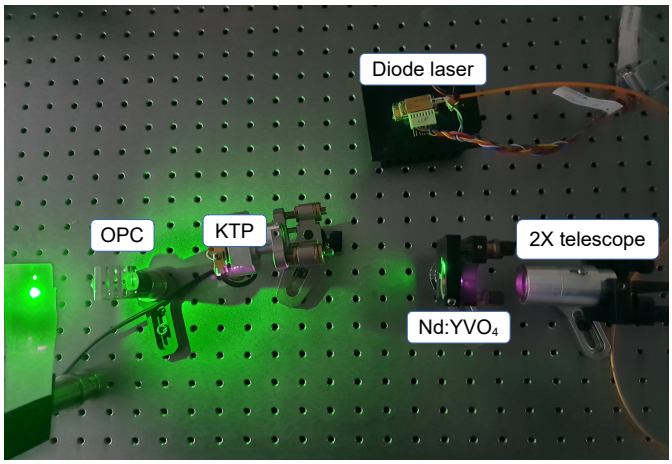

Figure 3.7: Photo of the intracavity SHG Setup

3.4 Results and discussion

3.4.1 *L-I* characteristics

The output green power (P_{SHG}) and the diode laser current (I_{LD}) are related as

$$P_{SHG} = SF(I_{LD} - I_{th})^2 \tag{3.2}$$

Where SF is the slope factor and I_{th} is the threshold current.

The laser diode current was varied and the output at 532 nm was measured using an Ophir 3A power meter. A nonlinear fit was done using equation (3.2) to determine the slope factor (SF = 75.8 $\pm$ 11.8 mW/A) and the threshold laser diode current (I_{th} = 0.42 $\pm$ 0.05 A).

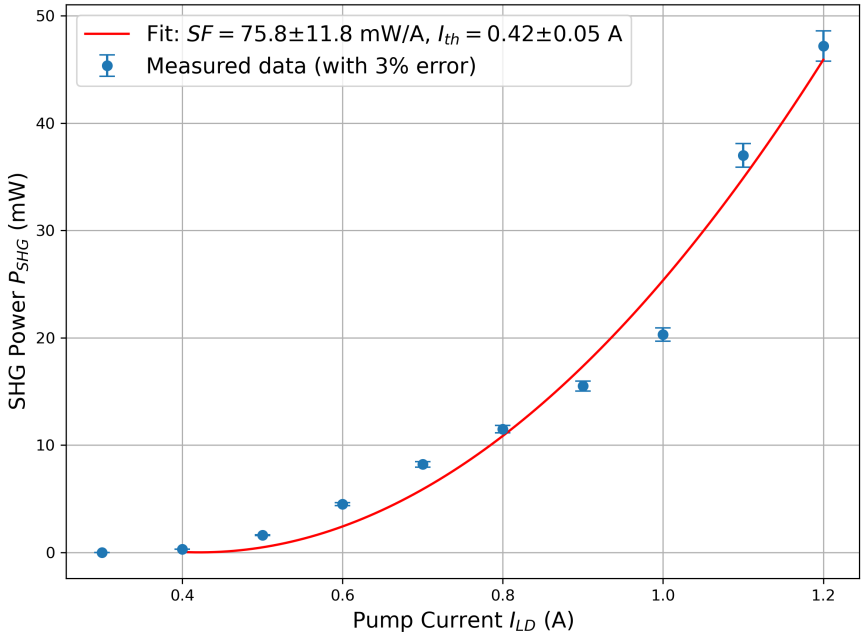

Figure 3.8: *L-I* characteristics plot of intracavity SHG laser

A SHG output of 47.2 mW was recorded at input diode current of 1.2 A with SHG-coupled IR output of 1 mW. Our requirement for the SHG power is 20 mW.

3.4.2 M^2 measurement

The M^2 parameter of the intracavity SHG source was measured using the knife-edge technique which is described in detail in 2.2.3. A focusing lens of focal length f = 75 mm was used to focus the beam.

This time, the M^2 parameter was measured in both vertical and horizontal directions. This is because, in this laser, a V-cavity is used where the beam is folded using a tilted

spherical mirror. Due to the tilt, astigmatism is introduced into the system which makes the beam shape elliptical. Therefore such an elliptical beam will have different M^2 parameter in different orientations.

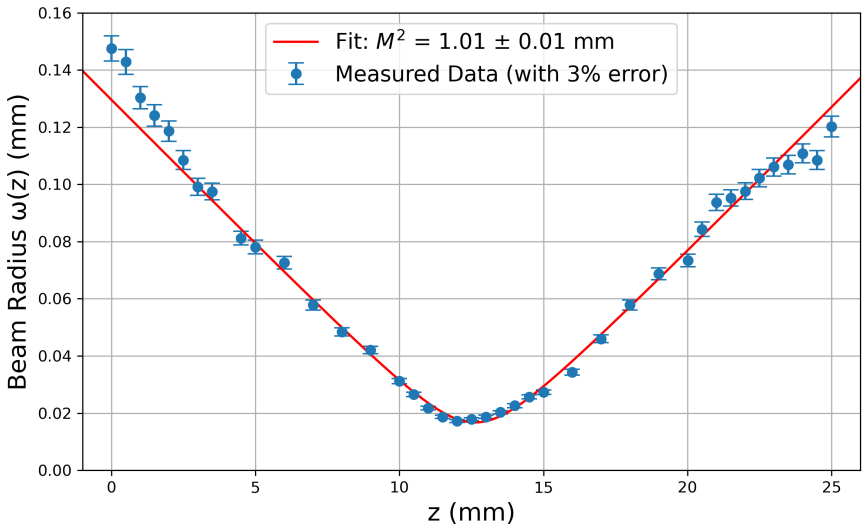

Figure 3.9: M^2 measurement of intracavity SHG laser in vertical

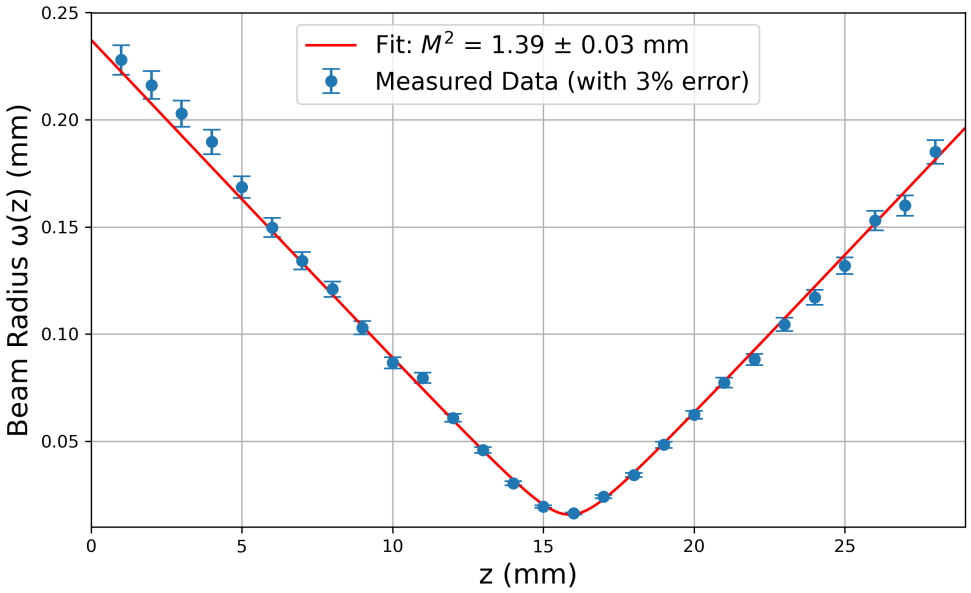

Figure 3.10: M^2 measurement of intracavity SHG laser in horizontal

It was observed that the beam was diffraction-limited (M^2 = 1.01 ± 0.01) in the vertical direction whereas the beam was nearly diffraction limited (M^2 = 1.39 ± 0.03) in the horizontal direction.

3.4.3 Variation of SHG power with temperature

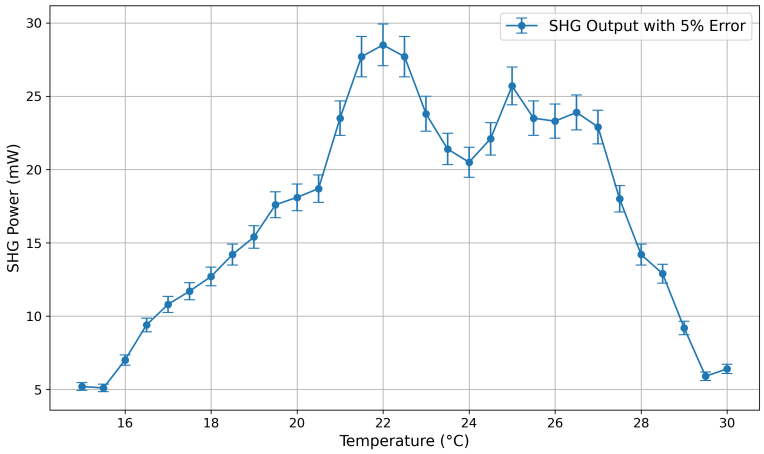

Figure 3.11: Plot of SHG power vs temperature for intracavity SHG laser

As shown in the plot, the maximum SHG power occurs at 22 °C, even though the nominal phase-matching temperature of the KTP crystal is 25 °C. Additionally, the temperature acceptance bandwidth was found to be approximately 9 °C.

3.4.4 SLM analysis

A scanning confocal cavity of finesse 200 and FSR 1.5 GHz was used to study the longitudinal modes of the SHG output.

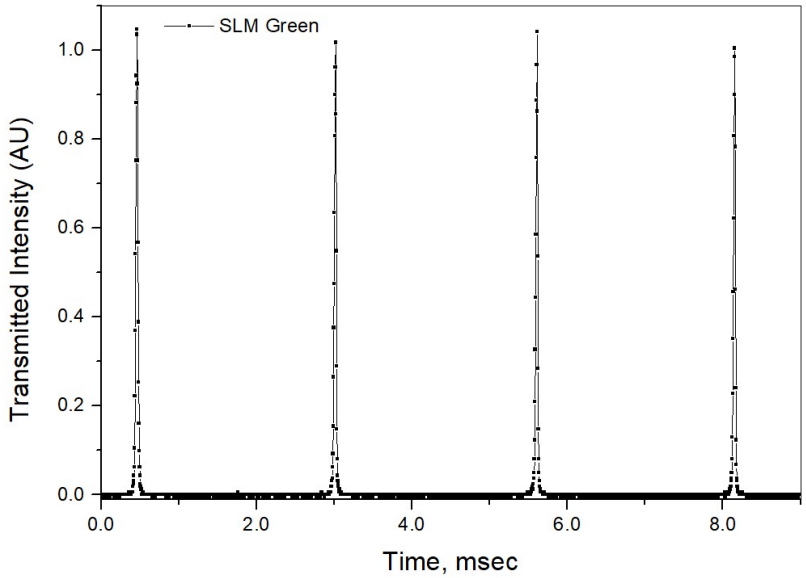

Figure 3.12: SLM plot for intracavity SHG laser

The transmitted signal from the photodiode was viewed on a DSO which shows single mode operation. The single mode operation in the intracavity mode is due to following effects:

- active etalon effect of the gain medium
- Gain reduction due to spectral and spatial dephasing in the presence of short absorption depth and spatial hole burning in the end pumped gain medium [14].

Chapter 4

External cavity SHG source at 532 nm using NPRO laser

This work is part of an ongoing departmental project at the Advanced Laser Development Lab (ALDL), RRCAT. While SHG sources for squeezed light at LIGO were based on linear cavity designs [15, 16], our approach employs a V-shaped external cavity.

4.1 SHG optimization

The first step is to optimize the SHG process and cavity parameters for maximum conversion efficiency.

The SHG power ($P_{2\omega}$) is related to crystal length (L), pump power (P_{ω}), and area of the pump beam (A_{ω}) through

$$P_{2\omega} \propto \frac{L^2 P_{\omega}^2}{A_{\omega}^2} \tag{4.1}$$

Here it is assumed that the temperature, angular, and spectral fluctuations for our KTP crystal are well within the corresponding acceptance bandwidths. Therefore, the dependence on the sinc function is neglected in the equation 4.1

A_{ω} Optimization

Condition: Crystal length $\approx$ Rayleigh range

$$L \approx z_R = \frac{\pi \omega_o^2 n}{\lambda} \tag{4.2}$$

For our KTP crystal, the effective L = 14 mm, n = 1.75, the optimum beam waist for λ = 1064 nm comes out to be $\sim$ **37** μm

P_ω Optimization

Condition: Input coupling at 1064 nm ≈ SHG conversion efficiency

Taking T_{in} (opt.) = 2.2%, $T_2 = T_3 = 0.2\%$ results in a cavity with finesse, $\mathcal{F} \sim$ **280**

4.2 V-cavity design and simulation

As in the intracavity case, reZonator v2.0.14 rc1 was used to simulate the V-cavity. Figure (4.1) shows the actual diagram of the V-cavity for external cavity SHG. Through this simulation, our aim was to find the values of d_1 and d_2 such that the beam waist inside KTP is close to 37 μm.

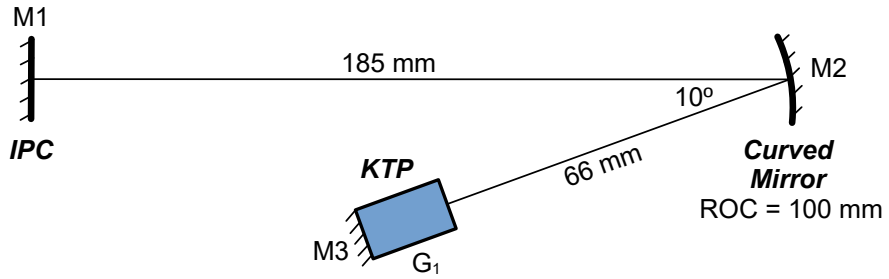

Figure 4.1: Schematic of the V-cavity used for external cavity SHG

Figure (4.2) shows the equivalent model of the V-cavity. In order to reduce complexity, the software reduces the two-arm cavity into a linear one by replacing the tilted mirror by a tilted lens. The underlying logic is that both systems exhibit nearly identical aberrations, such as astigmatism, with the primary difference being chromatic aberration. However, since we use an extremely narrow-linewidth (highly monochromatic) laser source, chromatic aberration becomes negligible.

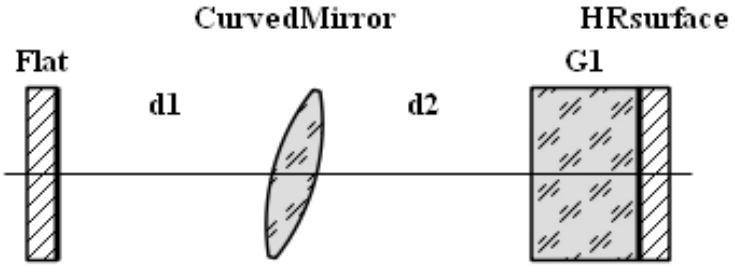

Figure 4.2: Equivalent model of the V-cavity used for external cavity SHG

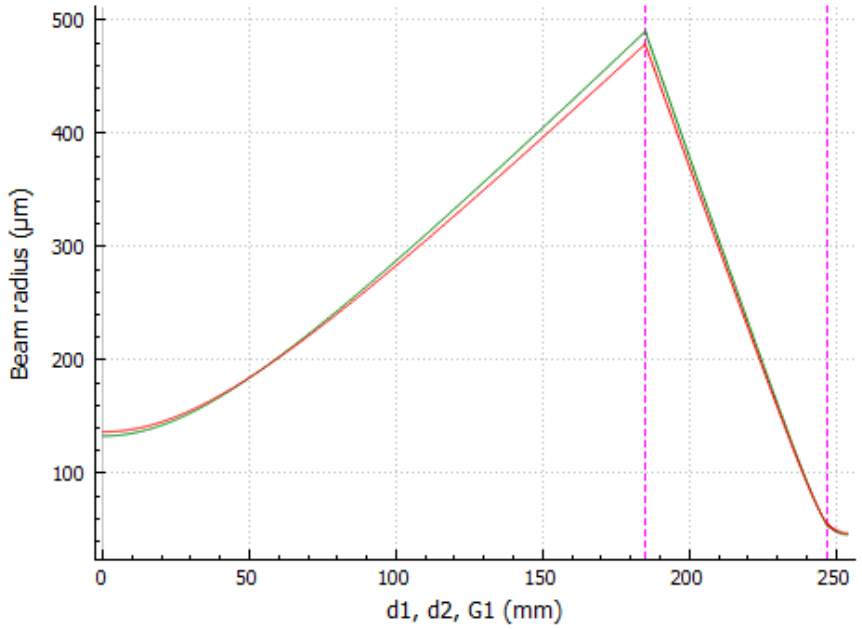

Figure 4.3: Cavity eigenmode of the V-cavity used for external cavity SHG

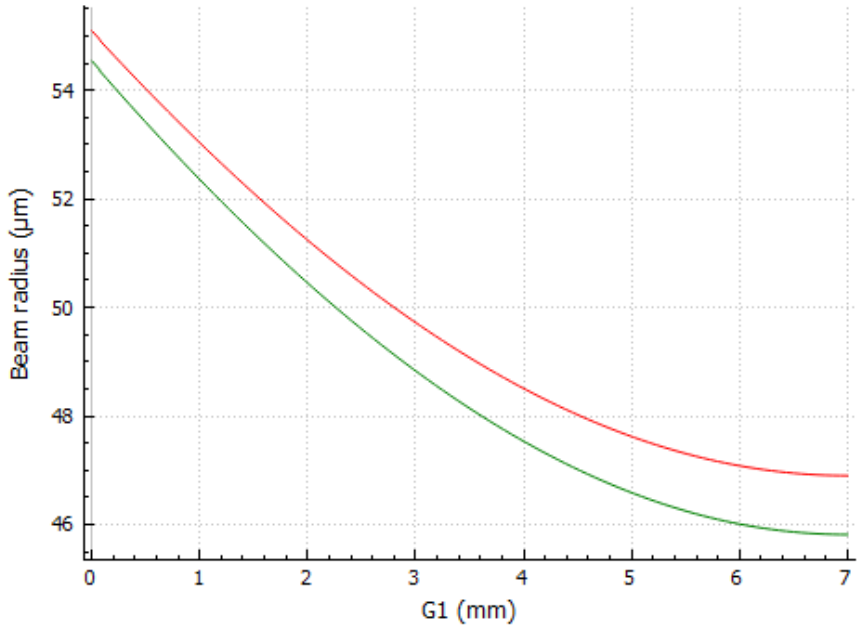

Figure 4.4: Beam waist inside KTP of the V-cavity used for external cavity SHG

Through simulation, it was found that for $d_1 = 185\,\text{mm}$ and $d_2 = 62\,\text{mm}$, the mean beam waist within KTP was approximately $46\,\mu m$ and the beam waist at the IPC was $135\,\mu\text{m}$.

4.3 Mode matching

Efficient coupling of a laser beam into an optical cavity requires good spatial overlap between the laser beam and the cavity's eigenmode. Therefore, mode matching is a critical step, especially in the external cavity configuration. Typically, two lenses are used for this purpose: one to collimate the laser beam and the other to focus it to the desired waist at the appropriate location. In our case, the beam waist of the eigenmode at the input coupler (i.e., 135 μm) was used as a target to determine suitable combinations of focal lengths for the mode matching optics.

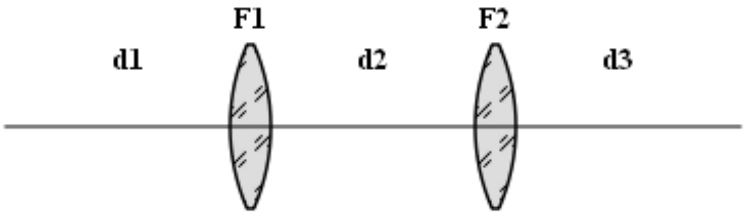

Figure 4.5: Setup for mode matching of external v-cavity and E-NPRO

For d1 = 205 mm, d2 = 350 mm and input waist (inside E-NPRO) $\approx$ 180 μm, collimating lens of f = 200 mm and the focus lens of f = 150 mm were found to be suitable for obtaining a waist of 135 μ m at d3 = 147.2 mm from the second lens.

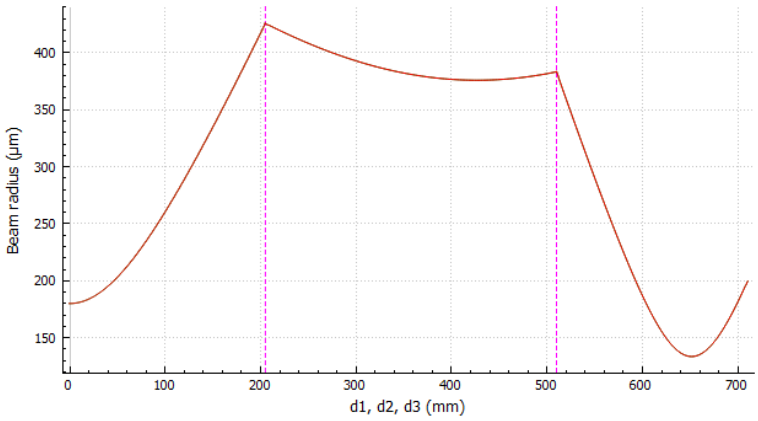

Figure 4.6: Beam simulation inside V-cavity used for external cavity SHG

To validate the simulation results, a knife-edge measurement was performed to determine the beam waist near the predicted waist location. The measured waist size was 134 μm, closely matching the simulated value of 135 μm. However, the waist position was found to be shifted by about 1.5 mm from the simulated location. This discrepancy is most likely due to the presence of optical components such as Faraday isolators and electro-optic modulators in the actual setup, which were not accounted for in the simulation that assumed only air between the lenses.

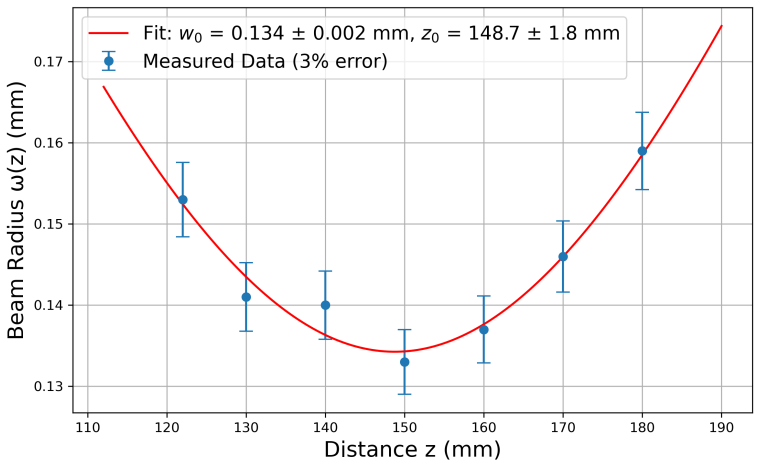

Figure 4.7: Beam waist and its location

4.4 Experimental setup

The laser used is an engineered version of NPRO (E-NPRO). QWP is a quarter wave-plate that converts an elliptically polarized beam from the E-NPRO to linearly polarized. Lens L1 is the collimating lens with a focal length of 200 mm. BS1 is a 90:10 beam splitter. The EOM and PD are part of the QubiG PDH controller. M1 is a HR mirror. BS2 helps limit the power to PD1 at 100 μW. The L2 lens is a focusing lens with a focal length of 150 mm. An additional half-wave plate (HWP) was used to rotate the vertically polarized beam to 45° for phase matching.

The beam from E-NPRO is phase modulated using the EOM which is driven by the local oscillator (LO) and the beam is incident on the input coupler (IPC) of the cavity.

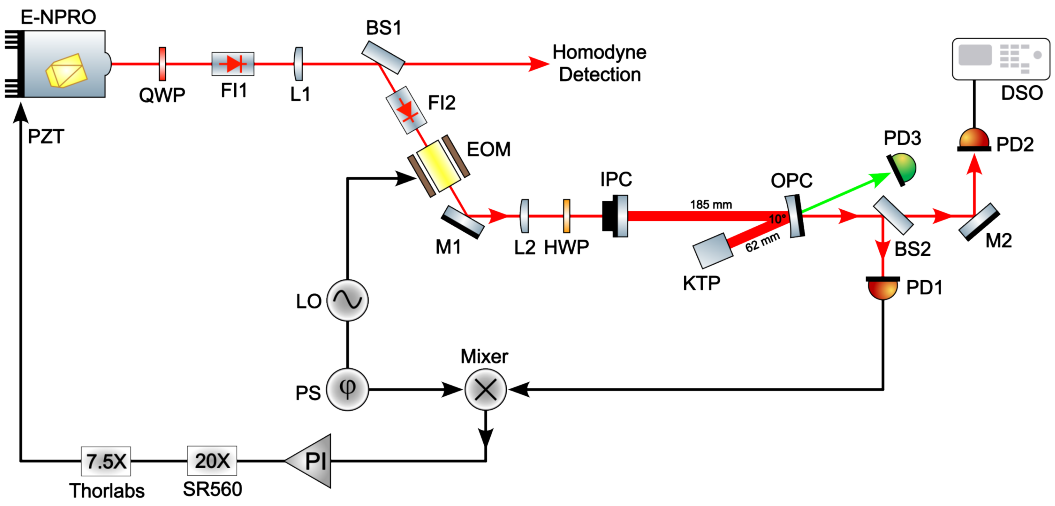

Figure 4.8: Schematic of the external cavity SHG laser

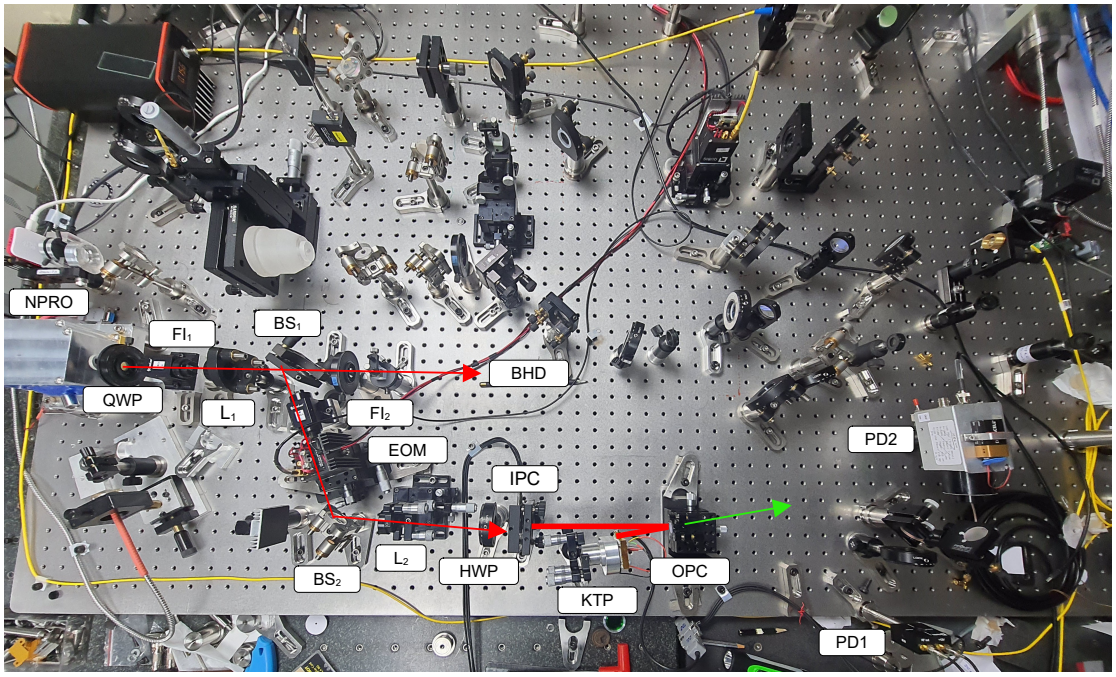

Figure 4.9: Photo of the external cavity SHG setup

4.5 Initial results

4.5.1 Waveplate effect and Polarization rotation

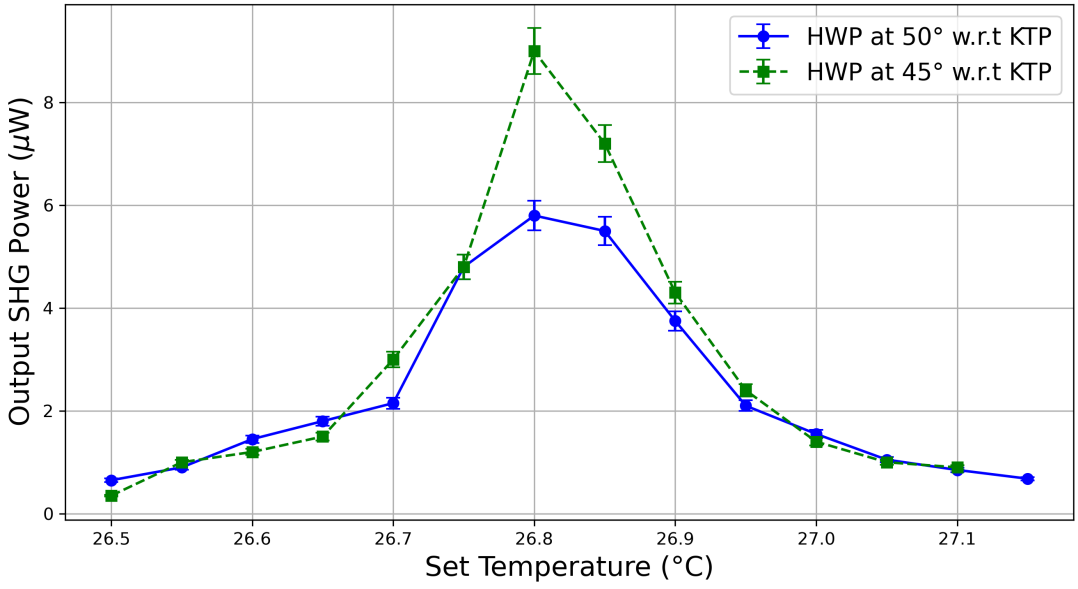

Figure 4.10: Plot showing variation of SHG power due to effect of variation in crystal temperature and HWP rotation.

From the plot, three key observations can be made:

- The SHG power reaches its maximum at 26.8 °C, rather than at the expected phase-matching temperature of 25 °C.
- The temperature acceptance bandwidth is extremely narrow, approximately 0.2 °C, which is even smaller than that observed in the intracavity configuration.
- The rotation of the half-wave plate (HWP) has a noticeable effect on the SHG power, indicating its influence on polarization alignment and phase matching.

4.5.2 Linear plano-concave cavity locking using transmission PDH

The KTP crystal was removed from the external cavity SHG setup, and the V-cavity cavity was repurposed into a plano-concave cavity to demonstrate transmission-based Pound-Drever-Hall (PDH) locking. The input coupler was a flat mirror with 2.2% transmission at 1064 nm, while the output coupler was a curved mirror with a radius of curvature (ROC) of 100 mm and 0.2% transmission at 1064 nm. The beam waist at the input coupler was approximately 130 μm, similar to that of the previously used V-cavity. The cavity had a free spectral range (FSR) of 3.2 GHz.

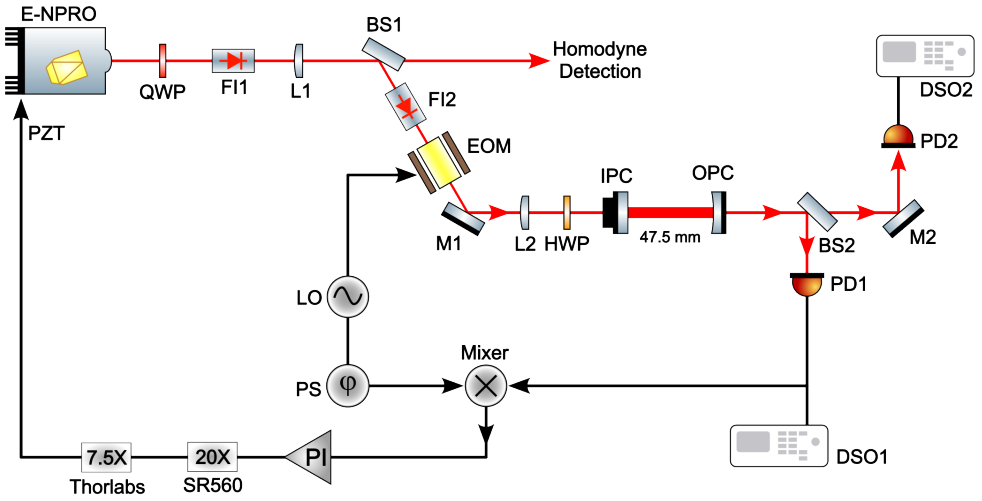

Figure 4.11: Schematic of the plano-concave cavity locking setup

The finesse of the cavity was estimated using the transmitted power. Resonance peaks measured with a photodiode (load resistance 100 kΩ) showed a peak voltage of 8 V. Assuming a photodiode responsivity of 0.1 A/W, the detected power was 0.8 mW. This corresponds to a circulating power of approximately 4 W, yielding a cavity finesse of about 126.

The cavity's transmission bandwidth was approximately 25 MHz. Since the phase modulation frequency was also 25 MHz, the sidebands fell within the transmission

bandwidth, preventing effective use of reflection-based PDH locking. Therefore, transmission PDH locking was employed. The transmitted signal was fed into a PDH mixer to generate the error signal, which was then amplified—first by a factor of 20 using a Stanford Research SR560 pre-amplifier, followed by an additional 7.5× amplification using a Thorlabs amplifier. The amplified error signal was then fed into the PI controller of the E-NPRO laser, successfully locking the laser to the cavity.

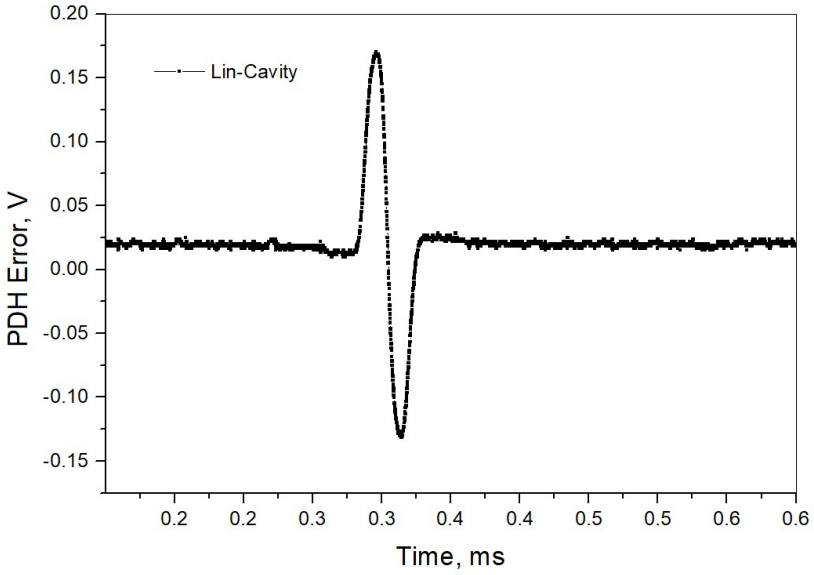

Figure 4.12: Plot of the Error signal (from DSO1)

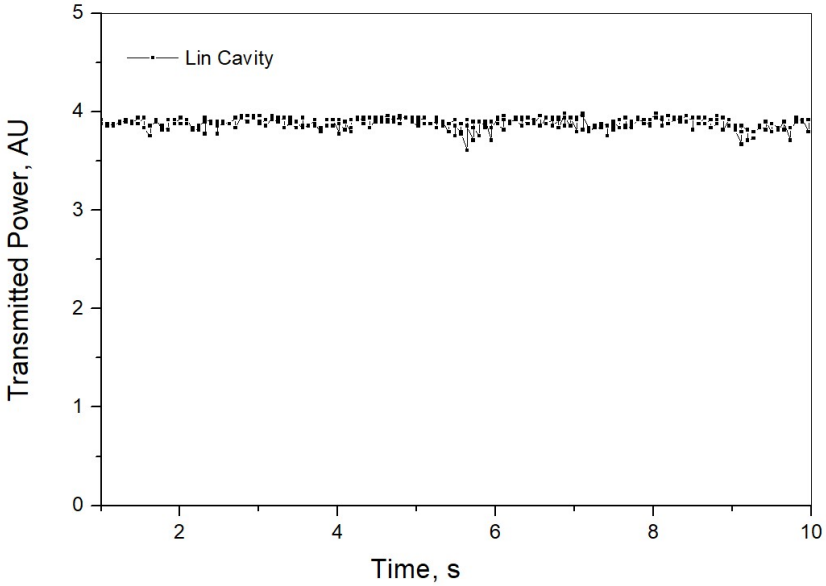

Figure 4.13: Cavity transmission after locking (from DSO2)

Chapter 5

Conclusion

The target SHG power of 20 mW was successfully achieved using the intracavity configuration. A maximum SHG output of 47 mW was obtained at a diode pump current of 1.2 A, corresponding to approximately 1 mW of SHG-coupled pump power. Beam quality measurements indicated an M^2 value of 1.01 ± 0.01 in the vertical direction and 1.39 ± 0.03 in the horizontal direction. Single longitudinal mode (SLM) operation of the laser was confirmed through spectral analysis of the SHG output. Additionally, the dependence of SHG power on the crystal temperature was investigated.

In the external cavity setup, the maximum SHG power achieved with 100 mW of pump power was only 150 μW—over 100 times lower than the desired target. The underlying causes of this low conversion efficiency are currently under investigation, and further studies are ongoing in this area. Some key studies included transmission PDH locking of the E-NPRO laser to the plano-concave cavity and an analysis of how variations in KTP temperature and polarization affect the SHG power.

References

[1] B. P. Abbott et al. Observation of gravitational waves from a binary black hole merger. *Physical Review Letters*, 116(6):061102, 2016.

[2] R. Smith. Theory of intracavity optical second-harmonic generation. *IEEE Journal of Quantum Electronics*, 6(4):215–223, 1970.

[3] A. Ashkin, G. Boyd, and J. Dziedzic. Resonant optical second harmonic generation and mixing. *IEEE Journal of Quantum Electronics*, 2(6):109–124, 1966.

[4] D.F. Walls and G.J. Milburn. *Quantum Optics*. Springer, 2 edition, 2008.

[5] Walter Koechner. *Solid-State Laser Engineering*, volume 1 of *Springer Series in Optical Sciences*. Springer, 7 edition, 2013.

[6] Thomas J. Kane and Robert L. Byer. Monolithic, unidirectional single-mode Nd:YAG ring laser. *Opt. Lett.*, 10(2):65–67, Feb 1985.

[7] Andri M. Gretarsson. *Optical Cavities*, page 133–151. Cambridge University Press, 2021.

[8] P. A. Franken, A. E. Hill, C. W. Peters, and G. Weinreich. Generation of optical harmonics. *Phys. Rev. Lett.*, 7:118–119, Aug 1961.

[9] Ronald WP Drever, John L Hall, Frank V Kowalski, James Hough, GM Ford, AJ Munley, and Hywel Ward. Laser phase and frequency stabilization using an optical resonator. *Applied Physics B*, 31:97–105, 1983.

[10] Eric Black. Notes on the pound-drever-hall technique. Technical Report LIGO-T980045-00-D, LIGO Project, 1998.

[11] Eric D. Black. An introduction to pound–drever–hall laser frequency stabilization. *American Journal of Physics*, 69(1):79–87, 2001.

[12] M. Nickerson. A review of pound-drever-hall laser frequency locking. Technical report, JILA, University of Colorado and NIST, Boulder, CO, USA, 2008.

[13] http://www.rezonator.orion-project.org/. Accessed: 21-05-2025.

[14] Jogy George. *A Study of Diode Pumped Solid State Lasers*. Phd thesis, Indian Institute of Technology (IIT) Mumbai, 2007.

[15] Sheila Dwyer. *Quantum Noise Reduction Using Squeezed States in LIGO*. Phd thesis, Massachussets Institute of Technology, 2013. Available from LIGO Document Control Center or institution repository.

[16] Simon Chelkowski. *Squeezed Light and Laser Interferometric Gravitational Wave Detectors*. Phd thesis, Gottfried Wilhelm Leibniz University Hannover, 2007. Available from LIGO Document Control Center or institution repository.